Overview and quality assessment of volcanic tuffs in the Mexican building heritage

Siegfried Siegesmund[1] · Christopher Pötzl[1] · Rubén López-Doncel[2] · Christian J. Gross[1] · Reiner Dohrmann[3,4] · Kristian Ufer[3]

Abstract

Many cultural heritage sites in Mexico have been built with volcanic tuff rocks from the earliest Central American civilizations to the time of the Spanish conquest and up to the present. Throughout this long period of time, the stones have been subjected to progressive weathering as evidenced by different types of damage phenomenon such as scaling, sanding, crumbling, sugaring and salt efflorescence. This study utilizes a collection of 53 tuffs from different regions in Mexico that show a diverse range of colors, rock compositions and mineralogy, and heterogeneous rock fabrics indicative of their volcanic origin. Comprehensive investigations have been done that include detailed petrographic analyses, cathodoluminescence, clay mineral analyses, and the determination of a wide range of petrophysical properties (e.g., porosity, capillary water uptake, water absorption, sorption, hydric and thermal expansion, and mechanical properties). All analyzed data combined are used for derivation of some general trends concerning the suitability/durability of tuffs applied as natural building stones.

Introduction

Volcanic rocks are one of the most used natural building stones, especially those known as tuffs or "tuff stones". These rocks have been used since the beginning of the first civilizations around the world in volcanic regions and are still abundantly applied today. Tuff deposits occur in great quantity as a result of their explosive volcanic origin. This has given rise to their great diversity in fabrics, colors, sizes and shapes of their clasts. Volcanic tuff rocks are relatively soft and easy to work with, and because of their diverse features they are attractive stones to use. Many people throughout human history have settled in volcanic areas and have used tuffs in large quantities to build all kinds of structures.

As designated by UNESCO, Mexico is one of the countries with the largest number of world heritage sites. Of these sites, the vast majority are constructions consisting of pyramids, colonial churches, or historical buildings, which were erected with natural stones (Fig. 1a–f). The stones used for the construction of these buildings were mostly rocks from the surroundings, so their lithology is dependent on the geology of each site.

Volcanic rocks have been used since the first cultures appeared in Mesoamerica. The earliest known Mesoamerican civilization, known as the Olmecs, began using and carving these stones more than 2000 years BCE. Pre-Columbian cultures used the rocks indistinctly for the filling of their pyramids, and looked for higher quality stones for the carving of their sculptures and ornamental pieces. The mastery of their carving techniques was in many cases so

✉ Christian J. Gross
  cgross@gwdg.de

1. Geoscience Centre of the University Goettingen, Goettingen, Germany

2. Geological Institute of the Autonomous University of San Luis Potosí, San Luis Potosí, Mexico

3. Federal Institute for Geosciences and Natural Resources (BGR), Hanover, Germany

4. State Authority of Mining, Energy and Geology (LEBG), Hanover, Germany

Fig. 1 Examples of different buildings and structures from the cultural heritage of Mexico built with volcanic stones. **a** Santo Domingo Temple, Oaxaca City (Cantera Verde tuff), **b** arches of the Faculty of Philosophy, Querétaro historical center (Escolásticas tuff), **c** Pyramid of the Sun, Teotihuacán, Mexico (basalts and andesites), **d** Government Palace, Mexico City center (Chiluca tuff), **e** facade in the historic center of Zacatecas (El Salto tuff), and **f** pavilion in the main square in the historical center of San Luis Potosí (Cantera Rosa tuff)

good that even very hard rocks such as basalt or andesite were used to carry out their ornamental works (Navarro et al. 2016). Many of the archaeological sites in Mexico were abandoned before the arrival of the Spanish in 1519. These structures suffered their greatest deterioration by natural physical, chemical, and biological weathering. Those still preserved were heavily damaged by the Spanish conquerors, or in many cases the pyramids were destroyed in order to build churches.

Later cultures, such as the Zapotecs, the Toltecs, the Aztecs, and others, developed in the north-central and central-southeast valleys of Mexico. They also utilized volcanic rocks for constructing the various structures in their cultures. For example, the Aztec people mainly settled in the central valley of Mexico, on what is geologically known as the Trans-Mexican Volcanic Belt (TMVB). The preferred building stones of the Aztecs consisted of basalts to rhyolitic ignimbrites, which they used for the construction of Tenochtitlan, the capital of their empire (López Luján et al. 2003; Mora-Navarro et al. 2016).

In Mexico, three important periods in the use of volcanic rocks can be defined as the pre-Columbian time, the colonization period and the modern-day application of these stones (Fig. 1a–f). Pre-Columbian cultures used all types of volcanic rocks, from very dense basalts and andesites to the easily reworked volcanic tuff rocks. Examples include the Pyramid of the Sun in Teotihuacán (Fig. 1c) or in the archaeological zones around the Templo Mayor in Mexico City (see Navarro et al. 2016; Wedekind et al. 2013). Buildings constructed with volcanic tuffs occur in Mitla, in the state of Oaxaca, or in the pyramids of Plazuelas in central Mexico (Pötzl et al. 2016).

During the period of colonization, under the cultural and religious influence of the Spanish, countless churches, monasteries, convents, and various colonial palaces were built, and unlike pre-Hispanic constructions, the Spanish preferred to use volcanic tuffs. For the foundations and wall-filling, various rock types were used without regard to their shape, color, or hardness. The Baroque architecture used in the new churches built in the New World required soft rocks that allowed the artistic carving of the facades. Thus, the artisans created works of great cultural value which can be recognized even today. The cities of Oaxaca, Guanajuato, Querétaro, Zacatecas and San Luis Potosí, among many others are all cultural heritage sites, which were erected with these types of rocks (Figs. 1, 2; Kück et al. 2020; López-Doncel et al. 2013, 2016, 2018; Wedekind et al. 2011, 2013).

After the first restoration works were carried out on the largest archaeological sites in the late 19th and early 20th centuries, the rocks were once again exposed and

Fig. 2 Deterioration phenomena in volcanic tuffs. **a** Cantera Rosa de San Luis Potosí, **b** column of Escolásticas tuff with marked efflorescence of salt causing loss of material and discoloration, inner courtyard of the Faculty of Philosophy in Querétaro, **c** scaling and chipping with structural disintegration of a column from a building in the historical center of Querétaro, Escolásticas tuff), **d** scaling and crumbling with loss of material, El Salto tuff, Zacatecas, **e** sanding in Cantera Rosa Oscura, San Luis Potosi, **f** scaling of Chiluca tuff, cathedral in Mexico City, and **g** scaling and sugaring, parallel to the lamination in the Loseros tuff, Guanajuato

began to show significant deterioration. Thus, restoration works were carried out periodically, utilizing the methods and techniques that existed at the time. This resulted in the detrimental restoration treatment of many ancient and historical structures and buildings. In these cases, the restoration products contribute to the deterioration of the rocks instead of helping to preserve them.

In recent years, the use of volcanic rocks as a building material has been increasing, mainly as decorative stones on floors, walls, and cladding, usually with very striking colors. A large number of new buildings, houses, and even streets and fences are built or decorated with these types of rocks throughout Mexico.

Given the great diversity and heterogeneity of volcanic tuffs, it is important to understand the mineralogical composition, the fabric, the petrophysical properties, and moisture aspects of the stones for making a good quality assessment. These different aspects also control the deterioration of the stone. Knowing the quality of the stone, the stone can then be applied as a construction element in various ways or be used for remediation work in the event of conservation and restoration work on monuments of cultural heritage.

Volcanoclastic rocks are extremely heterogeneous. Chemically they can go from basic to acidic. Texturally they can have various degrees of welding, different sizes and types of clasts, and a matrix that varies from vitreous

to crystalline, etc., so their responses to weathering can be very contrasting and unpredictable. Previous studies carried out on the volcanic rocks of some of these heritage areas have shown that the moisture properties are the main causes of deterioration (Fig. 2a–g), especially in the more porous variants (see Kück et al. 2020; López-Doncel et al. 2013, 2016, 2018; Pötzl 2020; Rucker et al. 2020; Wedekind et al. 2011, 2013). Some of these rocks are especially susceptible to deterioration caused by salt bursting and alveolar erosion, which causes a significant loss of material. The problems of hydric and thermal expansion are also equally well-known causes of deterioration (Fig. 2).

In this study, a large sampling of 53 volcanic tuffs from nine different states in Mexico was investigated and analyzed in the laboratory. The locations where the samples originate are shown on the geological map in Fig. 3. Such a large sampling allows us to make comparisons between the different tuffs, and based on the data accumulated, determine which tuffs can be used for specific purposes. This study only focuses on Mexican volcanic rocks; however, these rocks are also used as dimensional stones in Turkey, Hungary, Japan, South Korea, the Philippines, Italy, etc. (e.g. Fitzner 1985; Auras et al. 2000; Celik et al. 2014; Çelik and Sert 2020; Columbu et al. 2014; Germinario et al. 2017; Török et al. 2007, 2020; Pötzl et al. 2018a, b; Steindlberger 2003; Jo and Lee 2022).

Geological framework

The development and evolution of the various Mexican cultures over the centuries (pre-Columbian, colonization period to the present) have always gone hand in hand with volcanic activity. The rocks investigated in this study come from two different volcanic events that happened in the central portion of Mexico and these are associated with several factors, e.g. rifting and the interaction between several oceanic and continental plates from the Late Cretaceous to the present.

Some of the studied rocks belong to the first volcanic event and are exposed in the Mesa Central of Mexico. This is a region covered by Oligocene to Miocene volcanic fields of mainly rhyolitic volcanic rocks and is the southeastern termination of the Sierra Madre Occidental (SMO, Fig. 3).

Volcanism of this type is known to be related to pre-rifting magmatic events of continental regions undergoing extensive lithospheric extension such as the Basin and Range Province in North America (Bryan et al. 2002; Bryan 2007; Bryan and Ferrari 2013). Extension of the crust is proposed as the factor that favors the formation of large silicic magma volumes as it happened with the SMO (Brooks Hanson and Glazner 1995; Hildreth 1981; Wark 1991).

The Sierra Madre Occidental (Fig. 3) is the largest ignimbrite province in the world (Swanson and McDowell 1984) and the largest silicic igneous province in North America (Bryan and Ferrari 2013; McDowell and Keizer 1977). The SMO extends over more than 1200 km, in the north from the Basin and Range Province of the western part of the United
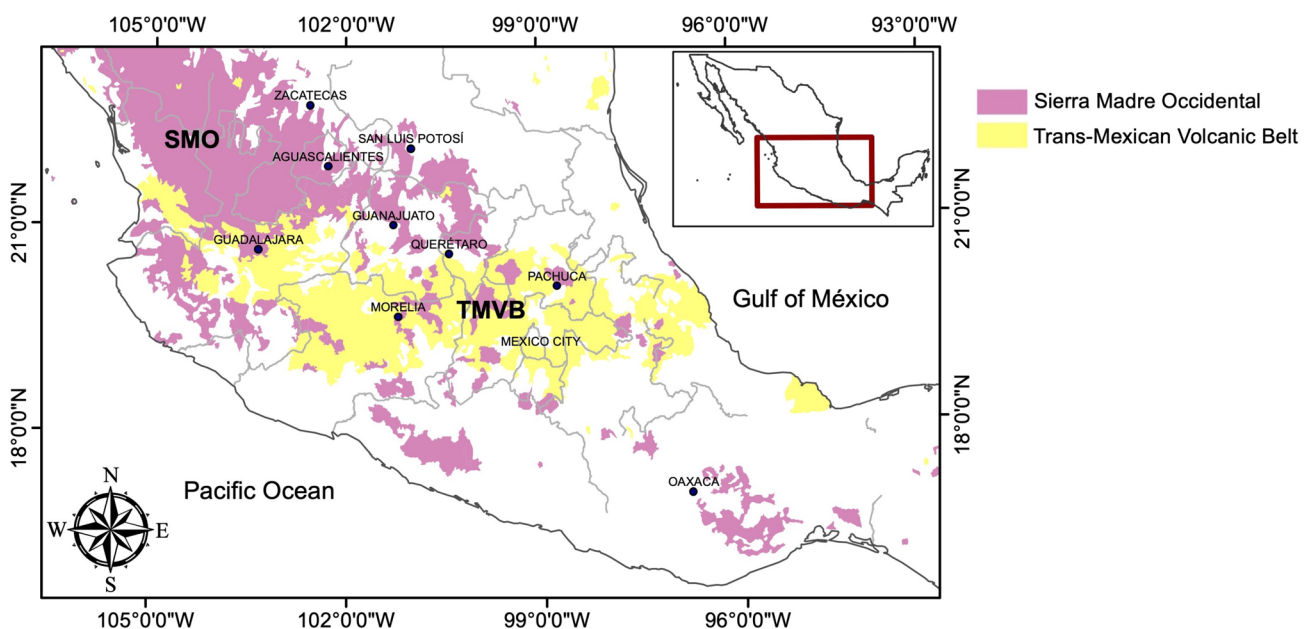
Fig. 3 Simplified geological map showing the Paleogene (pink) and Quaternary (yellow) volcanic fields (SMO, Sierra Madre Occidental and TMVB, Trans-Mexican Volcanic Belt) as well as the localities where the selected samples originate (modified from Padilla y Sánchez, 2017)

States to its intersection with the Trans-Mexican Volcanic Belt (TMVB) in the south (Sieck et al. 2019; Swanson and McDowell 1984). Most of the erupted rock volume of the SMO (85–90%) is represented by rhyolitic ignimbrites and the rest (10–15%) by rhyolitic lavas, domes as well as basaltic and andesitic lavas (Bryan and Ferrari 2013; Ferrari et al. 2018).

Mexico is part of the North American Plate that overrides the northern part of the Cocos Plate and the Rivera Microplate (Mori et al. 2009). This active plate boundary is related to Paleogene volcanism (Ferrari et al. 2012). It produced a second volcanic event associated with the Trans-Mexican Volcanic Belt (Fig. 3), a volcanic arc that crosses central Mexico from west to east (Pasquarè et al. 1991). Most of the examined tuffs in this investigation come from the TMVB.

The TMVB stretches to a length of about 1000 km from the Pacific coast through central Mexico and to the Gulf of Mexico. Its width ranges from 90 to 230 km. The TMVB is a Neogene volcanic belt that overlies the Cretaceous and Cenozoic magmatic provinces and has a heterogeneous basement. The basement is made up of terrains of different ages and lithologies. The volcanic belt was formed as a result of the subduction of the Cocos and Rivera plates under the North American continental plate (Ferrari et al. 2012).

The TMVB can be divided into the western, central, eastern, and easternmost sections. This classification is based on various properties such as subduction geometry, crustal thickness, the geology of the basement, and volcanic activities (Ferrari et al. 2012). The western and central sections, the basement of which was formed from the Guerrero terrain, are Mesozoic in age. The two eastern sections have a basement of Precambrian and Paleozoic ages, formed from the Mixteco and Oaxaca (eastern section) terrains and the Maya terrain (easternmost section) (Ferrari et al. 2012).

Materials and methods

Selected tuffs

In this study, 53 volcanic tuffs that are used as natural building stones in different geographic regions of Mexico (Fig. 3) were analyzed in regard to their petrography, mineralogy, petrophysical properties and weathering behavior. The samples were obtained from existing and abandoned quarries, waste stockpiles, from natural stone retailers and from buildings constructed with them. Wherever possible, samples were collected from the buildings, and if historical quarries still existed, they were also collected from these locations. These tuffs represent the great variability of building material exploited from the vast volcanic deposits in Mexico. From this large collection of tuffs, 12 representative tuffs were selected to be described petrographically in more

detail and investigated by the cathodoluminescence microscope (CL). Summarized petrographic descriptions of 48 tuffs are given in Table 1. In this collection, 32 samples were also analyzed geochemically, and 28 samples were analyzed by X-ray diffraction to determine the clay mineralogy and other phases (Table 2). The petrophysical properties for all 53 samples are given in Table 3.

Analyses of the petrography and petrophysical parameters

The microfabrics and mineralogical composition of 48 tuffs were investigated with a Zeiss Axio Imager.A2M petrographic microscope equipped with an Axiocam 305 color digital camera. Standard and polished thin sections 30 μm in thickness were used for the study. Many of the methods used below for determining the petrophysical properties in the tuffs are described in detail in Siegesmund and Dürrast (2011).

Cathodoluminescence (CL) microscopy is a useful tool for detecting different types of microstructures such as crystal zonations, discerning the mineralogical composition, and possible alteration features. The type of CL microscope applied in this study is the HC3-LM apparatus developed by Neuser et al. (1995), using an Olympus BHMJ microscope as its base. Operating conditions use a specimen vacuum chamber of 0.001 mbar, a filament current of 200 mA, and an accelerating potential of 14 kV. Since many of the investigated tuffs have a strong vitric component, the luminescence ranges from none to very low, thus longer exposure times are necessary. Twelve representative samples were selected. Descriptions concerning the technique of CL microscopy, theory, and application to geological materials can be found in Marshall (1988) and Machel et al. (1991).

X-ray diffraction (XRD) of whole rock samples and oriented slides of the clay fraction < 2 μm along with X-ray fluorescence (XRF) were used for the mineralogical and geochemical characterization of 28 tuff samples. They were supported by analysis of the cation-exchange capacity (CEC) analyses determined after the copper(II) triethylenetetramine method of (Dohrmann and Kaufhold 2009), modified from (Meier and Kahr 1999). A plausibility check of clay minerals was performed for all but three samples with a very low CEC, where insignificant amounts of expandable clay minerals can be expected. For sample CR-Gto no clay fraction could be separated because no sample material remained for analysis. Plausibility for this sample was checked with the Rietveld refinement of the XRD powder pattern instead, using the disordering models of Ufer et al. (2012).

The effective porosity σ (accessible to fluids and gases), the bulk (γ_b), and matrix (γ_m) densities were determined by hydrostatic weighing on sample cubes of 65 mm edge

Table 1 Compilation of 48 petrographically investigated tuffs, their classification, the TAS designation and a simplified summary of their macroscopic and microscopic features

Trade name and origin	Classification (Schmid 1981)	Classification (Fisher 1966)	Rock type (TAS)	Macroscopic characteristics	Microscopic features
Loseros (Los) Guanajuato (SMO)	Lithic tuff	Ash tuff	Dacite	Very fine laminations; green, reddish-brown or light gray in color; fine-grained, well-sorted volcanoclastic rock	Ash layers almost opaque; groundmass is v.f.g. crystallites; feldspars altered; relict shards; hypocrystalline to holohyaline fabric. Mostly lithic fragments of basalt/trachyte. Significant weathering & replacement by calcite + sericite + chlorite + epidote
Cantera Rosa (CR-Gto) Guanajuato (SMO)	Crystal tuff	Tuff	Dacite	Reddish-brown tuff with dominantly altered white lithoclasts; minor gray clasts and red scoria; lenticular & angular black fragments; matrix is v.f.g	Ash layers mostly opaque; hypocrystalline fabric; mm sized crystals are very broken; feldspars also broken as Kspar and plagioclase; large pore spaces due to weathered out clasts; matrix consists of v.f.g. crystals and altered crystals of v.f.g. crystals and altered crystals defined by dark brown extremely f.g. material (hematite); minor altered biotite? Devitrified clasts; dominant phase quartz
Cantera Hermosa Amarilla (CHA) Aguascalientes (SMO)	Vitric tuff	Tuff	Rhyolite	Yellowish tuff; fine-grained matrix; homogenous; mottled appearance due oxidation; black dendritic-like pyrolusite (?) appears on cut surface	Ash matrix essentially opaque; visible crystals show uniform grain size; fine-grained crystals are anhedral consisting of quartz and Kspar; relict glass shards (devitrified) visible in groundmass; XRD also indicates kaolinite as a major phase
Cantera Hermosa Rosa (CHR) Aguascalientes (SMO)	Vitric tuff	Tuff	Rhyolite	Light reddish to rosa-colored tuff; very homogenous fine-grained matrix; mostly dark clasts a few mm in size distributed evenly throughout	Tuff shows a hypocrystalline fabric; matrix essentially opaque; anhedral to subhedral Kspar and twinned plagioclase (around 7%); some crystals also broken; partially devitrified broken glass shards visible in the matrix; traces of diopside; quartz shows embayment features
Zacatecas Cathedral (ZaC) Zacatecas (SMO)	Vitric tuff	Lapilli tuff	Rhyolite	f.g, light pink tuff; Fe-staining; contains lithoclasts like collapsed pumice & scoria	Glassy (devitrified) fabric, essentially opaque. Fractured Qtz crystals with some embayments; lithoclasts altered
El Salto (ElS) Zacatecas (SMO)	Vitric tuff	Lapilli ash tuff	Rhyolite	Porous, bright reddish-orange tuff rich in crystals and lithoclasts	Hypocrystalline fabric; devitrified glass matrix. Crystals fractured to shattered and quartz shows some volcanic textures
Cantera Verde (CV) Oaxaca (SMO)	Crystal tuff	Ash tuff	Dacite	Light to dark shades of green, massive rock; considerable lithoclasts	Ash-rich hypocrystalline fabric; shard structures visible in matrix; devitrification of glass; lithic fragments are basalt & opaques; crystals fractured; indications of flow

Table 1 (continued)

Trade name and origin	Classification (Schmid 1981)	Classification (Fisher 1966)	Rock type (TAS)	Macroscopic characteristics	Microscopic features
Piedra Dura (PD n) Morelia (TMVB)	Vitric tuff	Lapilli tuff	Rhyolite	Massive rosa-colored tuff with a fine-grained matrix; white to light brown pumice clasts up to >40 mm also collapsed; clasts show an orientation; dark mm sized fragments show oxidation rings	Fabric is hypocrystalline with phenocrysts and fine-grained ash showing an alignment; crystals are broken consisting of quartz with embayments, twinned plagioclase laths; they are anhedral to subhedral; relict glass shards also occur showing recrystallization at the rims; XRD also identified smectite as a dominant clay mineral
Piedra Dura (PD a) Morelia (TMVB)	Vitric tuff	Lapilli tuff	Rhyolite	Same as PD n (fresh)	Same as the fresh variety; alignment of the broken anhedral to subhedral and euhedral crystals; Quartz and plagioclase are the dominant phases; groundmass essentially opaque with extremely fine-grained crystallites visible; relict glass shards occur along with fine-grained quartz and feldspar
Toba Rosa (TR) Plazuelas-Guanajuato (SMO)	Vitric ash tuff	Lapilli ash tuff	Rhyolite	Light brown to tan ignimbrite; grayish extremely flattened vesicular clasts; distinct flow orientation	v.f. micro-layering visible in ash-rich matrix; feldspar & quartz crystals aligned to flow direction. Clasts show recrystallization
Rosa Canada (RC) Queretaro (TMVB)	Vitric tuff	Tuff	Rhyolite	Medium red fine-grained tuff, rich in phenocrysts and lithic clasts showing black, gray, light gray and dark red colors; fragments are in the millimeter range	Hypocrystalline fabric where Kspar and twinned plagioclase phenocrysts are partially broken and anhedral to subhedral; slight alignment suggestive; groundmass essentially opaque in polarized light; relict glass shard fabric visible in the groundmass; minor higher birefringent mineral, amphibole? present
Escolasticas (ESC a) Queretaro (TMVB)	Vitric tuff	Lapilli ash tuff	Rhyolite	Light reddish brown tuff; numerous lithoclasts	Plagioclase clasts show rudimentary alignment. Crystals cracked and fractured. Ash-rich matrix almost opaque
Escolasticas (ESC n) Queretaro (TMVB)	Vitric tuff	Tuff	Rhyolite	Fine-grained porous tuff gray in color, numerous millimeter-sized clasts mostly gray to black with a few red cinder fragments	No thin section available
Cantera Rosa Obscura (CR ob) San Luis Potosi (SMO)	Crystal tuff	Ash-lapilli tuff	Rhyolite	Light to medium reddish brown, massive tuff containing lithoclasts; feldspar phenocrysts visible in hand specimen	Hypocrystalline fabric; unoriented feldspars supported by an ash-rich matrix

Table 1 (continued)

Trade name and origin	Classification (Schmid 1981)	Classification (Fisher 1966)	Rock type (TAS)	Macroscopic characteristics	Microscopic features
Cantera Rosa (en Monterrey, CR-Mty) San Luis Potosi (SMO)	Crystal tuff	Tuff	Rhyolite	Massive, dark rosa-colored tuff, porous, crystals consisting of quartz and feldspar, shows alignment and collapsed pumice clasts	Hypocrystalline fabric with a large percentage of very broken crystals of Kspar, plagioclase and quartz—anhedral to subhedral; parts of the groundmass is opaque; an alignment of the crystals is visible (flow texture); groundmass only partially opaque
Blanca Pachuca (BP) Pachuca de Soto (TMVB)	Crystal tuff	Lapilli ash tuff	Rhyolite	v.f.g light grayish tuff; lithoclasts present; strongly weathered pumice	Ash matrix is cryptocrystalline; fabric dominated by volcanic clasts. No distinct orientation to fabric
Rosa San Miguel el Alto (RSM) San Miguel el Alto (SMO)	Vitric tuff	Lapilli tuff	Rhyolite	Dark rosa colored tuff, fine-grained homogenous matrix; many elongated pumice clasts some > 1 cm in size; direction of flow also indicated, pumice clasts also weathered out; some mottling due to oxidation of Fe-rich lithic fragments	Rock shows a holohyaline fabric with only very coarser crystals of K-spar; groundmass is very fine-grained, which consists of anhedral quartz crystals and feldspar embedded in glass rich matrix; relict devitrified glass shards are evident indicated by very fine-grained crystals; opaques are also visible
Cantera Amarilla (CA) Guadalajara (TMVB)	Vitric tuff	Lapilli ash tuff	Rhyolite	Light to medium gray tuff; large variety of different lithic clasts e.g. vesicular scoria; flattened pumice show flow alignment	Pumice fragments show unique crystallization fabric (feather-like crystals); relict shards present; devitrification visible on shard rims
Cantera Gris (CG) San Miguel de Allende (TMVB)	Vitric tuff	Ash tuff	Trachyte	Brown, highly porous rock of low density. Occasional lithoclasts	Cryptocrystalline ash matrix; shards of broken glass; minor crystals; some pumice fragments
Gris Oscura Tuff (SG1) San Miguel de Allende (TMVB)	Crystal tuff	Lapilli ash tuff	Andesite	Dark tuff where the inclusions are black and coarse, which are embedded in a fine-grained brown matrix: the large percentage of plagioclase phenocrysts can be seen through the light reflected from cleavage surfaces; clasts range from mm to > cm in size	Hypocrystalline fabric consisting of numerous phenocrysts of twinned plagioclase, Kspar and quartz—anhedral to euthedral; plagioclase occurs as laths; some feldspars show zoning; some slight alignment of crystals can be discerned; some basaltic lithic clasts exhibit fine-grained, oriented laths of feldspar; groundmass essentially opaque, except for visible crystallites; crystals are also fractured; minor altered pyroxenes and olivine present

Table 1 (continued)

Trade name and origin	Classification (Schmid 1981)	Classification (Fisher 1966)	Rock type (TAS)	Macroscopic characteristics	Microscopic features
Gris Oscura Tuff (SG3) San Miguel de Allende (TMVB)	Crystal tuff	Ash tuff	Andesite	Brownish-gray tuff	Hypocrystalline fabric; large percentage of feldspar crystals (zoned feldspars), strongly fractured and broken; no orientations visible; opaque scattered throughout
Gris Oscura Tuff (SG4) San Miguel de Allende (TMVB)	Crystal tuff	Lapilli tuff	Andesite	More or less the same as SG1	Same as SG1 except that the crystals show a more uniform grain size; large lithic clasts also contain a hypocrystalline fabric where the groundmass is homogeneous and fine-grained; plagioclase occurs as laths showing twinning; feldspars also show zoning; groundmass in the clasts are opaque, whereas in the tuff proper extremely fine-grained crystallites are visible; distinct difference between ash-rich clasts and the main tuff fabric, i.e. the clasts are glassy and opaque, whereas the main tuff fabric is in part opaque but with numerous extremely fine-grained crystallites
Grey Tuff (GF1) San Miguel de Allende (TMVB)	Vitric tuff	Ash Tuff	Rhyolite	Can show a medium brown to dark gray matrix color, where the darker variety can show clasts in the mm to < cm size; fabric is slightly coarse in the lighter variety and in the darker type	Essentially a holohyaline fabric; shows an exceptional glass shard structure—opaque under polarized light and embedded in a devitrified matrix; minor crystals of quartz and feldspar (anhedral) indicate an orientation in the fabric; glass shards in the darker variety show a more distinct alignment
Grey Tuff (GF2) San Miguel de Allende (TMVB)	Vitric tuff?	Ash Tuff	Rhyolite	Same as GF1. Some pumice fragments	Similar to GF1 with a well-preserved shard structure
Red Tuff (RG1) San Miguel de Allende (TMVB)	Crystal tuff	Tuff	Andesite	Reddish-brown tuff containing medium-sized lithoclasts and smaller clasts in a fine-grained groundmass; crystals visible by light reflection on the feldspar cleavage planes	Hypocrystalline fabric with phenocrysts of twinned plagioclase, dominantly as laths and with periodic zonations; clasts are also crystal rich consisting of very fine crystals of plagioclase laths; some clasts are fine-grained ash and one identified to show a high percentage altered fine-grained mica; no distinct alignment in the crystals discernible; minor quartz is fine-grained

Table 1 (continued)

Trade name and origin	Classification (Schmid 1981)	Classification (Fisher 1966)	Rock type (TAS)	Macroscopic characteristics	Microscopic features
Red Tuff (RG2) San Miguel de Allende (TMVB)	Crystal tuff	Tuff	Andesite	Dark pink tuff with smaller clasts, gray to white around 0.5–1 cm in size embedded in an even finer-grained groundmass	Fabric and mineralogy similar to RG1; except this sample also shows the presence of olivine (?), partly altered
Red Tuff (RG3) San Miguel de Allende (TMVB)	Crystal tuff	Tuff	Andesite	Light pink tuff with a coarser grained groundmass	Fabric and mineralogy similar to RG1; smaller amounts of olivine than in RG2
Fachada Red Tuff (rTF) Zacatecas (SMO)	Vitric tuff	Tuff	Rhyolite	Fine-grained pink tuff with white, gray and brown lithic clasts up to 5 mm in size; a weak gradation is visible	Hypocrystalline fabric where a cryptocrystalline matrix makes up more than half of the rock, along with very fine grained quartz and feldspars; Minor relict devitrified shard structures are observable; contains < 1% coarse crystals consisting of quartz and altered feldspars and also opaques
Cantera Red Tuff (rTC) Zacatecas (SMO)	Vitric tuff	Tuff	Dacite	Red tuff with a high content (around 15%) of phenocrysts and lithic clasts up to 2 mm in size; white clasts are weathered; slight orientation of the clasts visible	Hypocrystalline tuff containing around 2% coarse anhedral quartz with embayments and feldspar crystals, some showing alteration; dominant matrix is cryptocrystalline which is widely stained by reddish brown hematite; minor opaques
Orange Lapilli Tuff Konvent (oLtK) Zacatecas (SMO)	Lithic tuff	Lapilli tuff	Dacite	Porous tuff with an orange groundmass, includes around 40% lithoclasts	Dominant phases are quartz in the ash-rich and glassy matrix; minor coarser recrystallized quartz is also evident; muscovite—illite associated with the many lithic clasts of weathered lava; some of the clasts are cryptocrystalline, possibly rounded pumice; biotite clasts and minor epidote; fabric is hypocrystalline but shows no visible orientation
Violet Lapilli Tuff La Cueva (LC) Zacatecas (SMO)	Vitric tuff	Lapilli tuff	Rhyolite	Violet porous tuff with a high percentage of white lithic clasts and greyish pumice clasts	No thin section available XRD: major phases cristobalite/tridymite and kaolinite; quartz & alunite are minor phases; traces of diopside

Table 1 (continued)

Trade name and origin	Classification (Schmid 1981)	Classification (Fisher 1966)	Rock type (TAS)	Macroscopic characteristics	Microscopic features
White Tuff Blanca de Jerez (BJ) Zacatecas (SMO)	Vitric tuff	Tuff	Rhyolite	Porous white tuff; numerous mm-sized lithoclasts ranging in color from dark red to gray to black; some pumice fragments	Very fine-grained hypocrystalline fabric with <1% coarser crystals of feldspar: the dominant groundmass (XRD analyses) consists of quartz and Kspar; both the glassy component and the extremely fine-grained crystals make up the dominant fabric; major components also include the clay minerals smectite and kaolinite (XRD)
Whitish–violet Tuff La Quemada (TLQ) Zacatecas (SMO)	Vitric tuff	Tuff	Dacite	Tuff with a white and violet coloration, lithic clasts are red, indented pumice clasts	Dominant fabric consists of ash-rich glassy material, essentially opaque in thin section; evenly distributed throughout are also extremely fine-grained microlites probably the result of the devitrification process; around 2% coarser anhedral feldspar and quartz occurs; pumice clasts consists of both a glassy component and a fine-grained component of quartz and feldspar(?) with a greater grain size than the groundmass; indications of relict glass shards can be discerned in the groundmass
Rosa Lapilli Tuff Puerta Chula (PC) Zacatecas (SMO)	Vitric tuff	Lapilli tuff	Rhyolite	Massive tuff pink in color containing pumice clasts in the cm range, few lithic clasts; flattened and elongated tuff clasts indicate a flow direction	Dominant fabric surrounding the flattened pumice clasts hypocrystalline; under transmitted light a flow direction is partially discernible; relict shard structures are also observable under transmitted light; recrystallization of the extremely fine-grained ash component is also visible. XRD analyses indicate quartz and smectite being the dominant phases, followed by feldspar; traces of mica visible in thin section and identified by XRD as muscovite-illite; hematite also occurs as a trace reddish accessory mineral

Table 1 (continued)

Trade name and origin	Classification (Schmid 1981)	Classification (Fisher 1966)	Rock type (TAS)	Macroscopic characteristics	Microscopic features
Brownish Tuff Susticacán (SU) Zacatecas (SMO)	Vitric tuff	Tuff	Rhyolite	Fine-grained light reddish-brown porous tuff; very minor lithic clasts	Hypocrystalline fabric consisting of relatively even proportions of a glass and crystalline components; dominant phase is quartz followed by Kspar; tuff also exhibits an excellent glass shard structure; shards also show a feather-like structure, where crystals have grown perpendicular to the shards rim; between these shard fine grained anhedral quartz occurs; traces of hematite were detected by XRD
Salmon-colored Lapilli Tuff Batida (BE) Zacatecas (SMO)	Vitric tuff	Lapilli tuff	Rhyolite	Salmon-colored, highly porous tuff, pumice clasts occur in the cm range, also small lithic fragments; Some clasts partially replaced by sericite with a glassy structure, probably pumice fragments	Very fine-grained tuff with a hypocrystalline fabric; contains around 3–5% coarse phenocrysts of quartz (embayed) and feldspar is fractured with sericite associated with the fractures; matrix is ash-rich and essentially opaque in thin section; quartz dominates as the main phase followed by feldspar and smectite (XRD analysis); minor muscovite occurs as visible flakes in thin section; biotite crystals also replaced by chlorite. Hematite expressed as a secondary mineral
Zacatecas (SMO)	Vitric tuff	Lapilli ash tuff	Rhyolite	Tuff gray in color, numerous white clasts, also gray pumice clasts	Large quantity of fine-grained clasts evenly distributed throughout, especially visible in transmitted light; around 3% of anhedral feldspar phenocrysts; fabric is hypocrystalline of very fine-grained opaque ash and very fine-grained crystals of quartz (the dominant phase); XRD also indicates kaolinite as a dominant component, whereas hematite occurs as a minor phase; clasts are essentially cryptocrystalline

Table 1 (continued)

Trade name and origin	Classification (Schmid 1981)	Classification (Fisher 1966)	Rock type (TAS)	Macroscopic characteristics	Microscopic features
Orange Tuff Fresnillo (FR) Zacatecas (SMO)	Vitric tuff	Tuff	Rhyolite	Fine-grained orange tuff, visible feldspar crystals and pumice clasts	Hypocrystalline fabric with around 3% of phenocrysts consisting of feldspar anhedral to euhedral; these are embedded in a very fine-grained ash-rich/glassy matrix—mostly opaque in thin section; some of the feldspar (Kspar) show evidence of alteration; the very-grained quartz (dominant phase) in the matrix is anhedral; XRD indicates kaolinite is also a major component; some relict shards
Ignimbrita Escolásticas Gris (TGQ) Queretaro (TMVB)	Vitric tuff	Tuff	n.d	Medium brown tuff with a faintly discernible fine lamination	Hypocrystalline fabric with phenocrysts of plagioclase laths showing a distinct flow direction orientation; plagioclase is twinned, some zoning visible and they are fractured and broken; groundmass is a very fine-grained ash-rich and glassy material, where devitrified relict glassy shards are still visible
Ignimbrita Rosa de la Canada del Marques (TRCQ1) Queretaro (SMO)	Vitric tuff	Lapilli tuff	n.d	Light reddish brown tuff with flattened and elongated tuff clasts from a few mm to > 1 cm in size; also includes a variety of lithic clasts showing dark red, grey and black colors from a few mm to > 5 mm	Hypocrystalline tuff that shows a variety of complex fabric structures, e.g. pilotaxitic fabric where aligned plagioclase laths flow around twinned coarse phenocrysts of plagioclase; devitrified components in pumice clasts that show feathery-like crystal growth structures; xenoliths of volcanic rock fragments; feldspars that show sieve structures; broken glass shards that also show complex recrystallization structures; lithic clasts with altered mica crystals
Toba gris de la Alberca original (TGCAQO) Queretaro (SMO)	Vitric tuff	Ash Tuff	n.d	Medium brown tuff with minor lithic clasts but crystal phenocrysts that reflect light from feldspar cleavage surfaces; indications of very fine laminations	Overall fabric is hypocrystalline where the phenocrysts show alignment; consists of angular, broken twinned plagioclase, some showing sieve structure; altered olivine inclusions in twinned plagioclase phenocrysts (?); possible minor pyroxene; quartz shows some embayment; matrix shows relict glass shards showing devitrification from their rims and oriented parallel to the observable micro-lamination

Table 1 (continued)

Trade name and origin	Classification (Schmid 1981)	Classification (Fisher 1966)	Rock type (TAS)	Macroscopic characteristics	Microscopic features
Ignimbrita Roja de Huimilpan (TRH) Queretaro (TMVB)	Vitric tuff	Tuff	n.d	Dark reddish brown tuff, very fine-grained matrix with dark gray lithic fragments; fine crystal phenocrysts are visible by light reflecting off feldspar cleavage planes	Overall fabric shows distinct flow orientation by aligned feldspar phenocrysts and in thin section scans, the devitrified glass shards are also aligned; plagioclase shows twinning; also minor altered pyroxene, some occur as inclusions in feldspar; glass and ash-rich matrix is essentially opaque; rims of the glass shards indicate devitrification; lithic fragments show alteration
Ignimbrita Amarilla de Huimilpan (TAH) Queretaro (TMVB)	Vitric tuff	Tuff	n.d	Light medium reddish brown tuff, very fine-grained matrix with <mm to 1 mm lithic fragments and crystal phenocrysts evident by light reflecting off feldspar cleavage surfaces	Rock fragment similar to TRH: plagioclase laths and lithic fragments show alignment as well as the devitrified glass shards visible in thin section scans; glass shards show recrystallization with crystal growth perpendicular to the shard rim; plagioclases shows typical twinning and sieve structure; minor poikioblastic orthopyroxenes are altered; lithic fragments also show alteration to clay minerals (?); minor opaques, probably hematite
Ignimbrita Colón (WT) Queretaro (TMVB)	Vitric tuff	Lapilli tuff	n.d	Light gray, low density probably due to a higher porosity similar to pumice, overall most of the clasts have a color similar to the matrix, although some are brown to gray and range from a few mm to around 1 cm	In thin section scan the lapilli show partially chaotic fabrics to strongly aligned fabrics where the microscopic components are flattened; very minor plagioclase phenocrysts (some zoned); the matrix is in part cryptocrystalline and made up of strongly oriented stretched glass, which also show alteration (?) to high birefringent clay minerals; these stretched glass structures are opaque; another almost opaque phase associated with the stretched glass form augen-shaped crystals, possibly altered glass

Table 1 (continued)

Trade name and origin	Classification (Schmid 1981)	Classification (Fisher 1966)	Rock type (TAS)	Macroscopic characteristics	Microscopic features
Ignimbrita Escolásticas Negra, Querétaro (BT) Queretaro (TMVB)	Vitric tuff	Lapilli tuff	n.d	Tuff with a dark brown, very fine-grained matrix that includes various lithic components showing gray, medium reddish brown to black colors with sizes ranging from <1 mm up to >1 cm	Matrix is a fine-grained ash with a glassy component (shard structure not evident), some lithic clasts appear recrystallized and contain very fine-grained (?) clay minerals; some clasts show a pilotaxitic fabric; quartz has undergone recrystallization in some parts of the fabric; calcite also occurs as a minor mineral; biotite and muscovite may both occur, where biotite shows alteration to chlorite (green colors in transmitted light); twinned plagioclase phenocrysts show alteration; opaques occur throughout the fabric
Cantera Blanca de Las Palmas (LPW) Queretaro (TMVB)	Vitric tuff	Tuff	n.d	Very dense, light yellowish white tuff, almost porcelain-like which is extremely fine-grained and homogeneous	Extremely fine-grained hypocrystalline fabric; some relict shard-like structures visible in transmitted light, which shows an orientation (micro-lamination); crystalline component dominates (quartz and feldspar)
Cantera Roja de Tierra Dura (TDW) Queretaro (TMVB)	Vitric tuff	Tuff	n.d	Extremely fine-grained, light yellowish white tuff, somewhat dense and similar to LPW, but elongated and flattened vugs with lengths of around 5 mm and widths < 1 mm occur – these are oriented indicating a weak lamination structure	Tuff shows a uniform grain size in thin section; hypocrystalline fabric; the only larger crystals consist of quartz, and they occur in the vug spaces exhibiting crystal growth from rim to core; these quartz crystals also show a sieve structure
Chiluca Tuff (CH) Mexico City (TMVB)	Crystal tuff	Ash tuff	Andesite	Gray tuff with mafic and felsic lithoclasts	Similar to Gris Oscura; hypocrystalline fabric; crystals embedded in ash-rich matrix; feldspars zoned, fractured and broken; crystals show strong alteration; no orientation of crystals evident. Hornblende and minor pyroxene occurs

Left column also indicates their location and assignment to the SMO (Sierra Madre Occidental) and the TMVB (Trans-Mexican Volcanic Belt; see geologic map in Fig. 3)

f.g. fine-grained, *v.f.g.* very fine-grained, *n.d.* not determined

Table 2 Mineralogical composition of the tuffs investigated—cation exchange capacity (CEC), clay minerals and other phases

Sample	CEC (meq/100 g)	CEC confirmed by clay mineralogy	Clay minerals									Zeol.	Other minerals											
			Smectite	Vermiculite	Illite-smectite (R0)	Illite-smectite (R1)	Illite-smectite (R3)	Illite-smectite (1:1, irregular)	Muscovite/illite	Kaolinite	Halloysite	Clinoptilolite	Quartz	Cristobalite/tridymite	Glass	Calcite	K-feldspar	Plagioclase	Hornblende	Gypsum	Alunite	Diopside	Hematite	Anatase
Los	18				XXX			XXX	+	+			XXX	X		XX	XX	XX						
CR-Gto	25		XXX						+				XXX			X	XX	XX					+	
CHA	5				X				+	XXX			XXX				XX	+						+
CHR	4												X	XXX			XXX	XXX					+	
ZaC	11					XX							XXX	X			+			+			+	
EIS	5	<2 µm	XX				XX		+	XXX			XXX	+			XXX			+			+	
CV	5	zeolite							+			XXX	XXX											
PD n	4	<2 µm	XXX		X				+	X			XXX	XXX			XXX	XXX					+	
PD a	2				X				+				XXX	XXX			XX	XXX					+	
RC	1				X								X	XXX			XXX	XXX						
ESC a	1												+	XXX			XXX	XXX	+				+	
ESC n	1												+	XXX			X	XXX	+				+	
CR ob	2				+				+	XXX			XXX	XX			XX	XXX					+	
CR-Mty	1				+				+	XX			XXX	+			XXX	XXX					+	
BP	5	<2 µm					XXX		+				XXX				+	XXX						
CA	5	<2 µm	XXX							X(?)	X(?)		X	XXX		X	XX	XXX						
CG	3		X										XXX		XXX		XX	XXX						
rTF	13			X?		XXX							XXX				X			+			+	
rTC	13			X?		XXX				XX			XXX										+	
oLT	2			X?						X			XXX	+			XX						+	
BJ	7	<2 µm	XX							XX			XXX	+			XXX						+	
TLQ	2									XXX			X	XXX			XXX				X	+	+	
PC	18		XXX						+				XXX	XX			XX						+	
SU	1				+								XXX				XX						+	
BE	12		XX						+	X			XXX	+			XX						+	
SC	3								+	XXX			XXX				XX						+	
FR	1									XXX			XXX	+			+							
oLK	4							XXX					XXX				XX						+	

XXX dominant mineral phase, XX major component, X minor component, + trace phase

length after DIN 772-4 (1998). The pore radii distribution of the samples was determined on sample fragments after DIN 66133 (1993) by mercury intrusion porosimetry (MIP) using low (PASCAL 140) and high pressure (PASCAL 440) units from Thermo Fisher Scientific.

The determination of maximum capacity of water absorption W_{vac} was determined by the weight difference of the dry and fully water saturated sample cube of 65 mm edge length under forced (vacuum) conditions for 24 h. The voluntary water absorption W_a was determined under atmospheric conditions. The quotient of both values is described by the dimensionless saturation coefficient S and allows for the estimation of the frost resistance of the stone according to Hirschwald (1912).

The w value (capillary water uptake) was determined according to the DIN EN ISO 15148 (2003) in a closed cabinet while weighing over time. The dry sample cube of 65 mm edge length was attached to an under-floor balance and in minimal surface contact (≤ 5 mm) with a bath of demineralized water and subsequently weighed over time. The dimensionless coefficient of water vapor diffusion resistance (μ) characterizes the diffusion resistance of the material towards the moisture of the adjacent air (Siegesmund and Dürrast 2011) and was determined according to the DIN EN ISO 12572 (2017) with the wet cup method.

The hygroscopic water sorption describes the amount of water that the specific surface area of the pores adsorbs from the air. It was determined on oven dried (40 °C for 7 days) cylindrical samples of 15 mm diameter and 50 mm length in a climate chamber (Feutron KPK 400) at a temperature of 23 °C with a stepwise increase of the relative humidity (RH) from 25 to 95% according to the DIN EN ISO 12571 (2013). Due to time constraints (constant mass due to high ratios of micropores can only sometimes be reached after weeks), the humidity was increased by 10% every 48 h while determining the weight difference before every humidity increase.

The ultrasonic P-wave velocity was determined via direct transmission of the ultrasonic travel time through a respective travel distance according to the DIN 14579 (2005) (with a frequency of 350 kHz). By means of the Brazil test (or indirect tensile strength test; DIN 22024 (1989)), the tensile strength (TS) was measured on disc-shaped specimens of 20 mm in length and 40 mm in diameter. In order to identify the anisotropic behavior of the tuffs, the TS was determined parallel (X direction) and perpendicular (Z direction) to the bedding plane, on a minimum of six specimens per direction.

The hydric expansion was measured on cylindrical samples of 50 mm length and 15 mm diameter under conditions of complete immersion in demineralized water following DIN 13009 (2000). A displacement transducer with a resolution of 0.1 μm measured the linear expansion as a function of time. The thermal expansion behavior was determined in a climate chamber via a pushrod dilatometer and displacement transducer with a resolution of 0.1 μm following DIN EN 14581 (2014) and expressed by the coefficient of thermal expansion α. The cylindrical samples of 15 mm diameter and 50 mm length were exposed to two heating and cooling cycles under dry conditions. In each cycle, the oven dried samples (40 °C for 7 days) were heated from 20 to 90 °C and subsequently cooled down to 20 °C, with a heating/cooling rate of 1 °C/min. Both minimum (20 °C) and maximum (90 °C) temperatures were held for 6 h.

The salt weathering resistance of the investigated tuffs was determined by a cyclic salt weathering test, based on the standard DIN EN 12370 (2020) on cubes of 65 mm edge length. For one cycle of the test, the dry cubes were put in a 10% solution of sodium sulfate (Na_2SO_4) for 4 h. The samples were dried afterwards in an oven (60 °C) for 24 h and subsequently weighed. This process was repeated until a minimum weight loss of at least 30% was achieved.

Results and discussion

Mineralogical and geochemical characterization

The stones selected for the detailed petrographic investigation represent a diverse collection of pyroclastic rocks showing a wide range of fabrics, microstructures, grain sizes, volcanic clasts, and mineralogical composition (Figs. 4, 5). These rocks are characterized by an ash-rich matrix or ones with a significant glass content (e.g., glass shards). Other stones are classified as crystal tuffs, e.g., the Chiluca tuff with visible plagioclase and hornblende phenocrysts, or as a lithic tuff like the laminated Loseros tuff. These twelve representative candidates are described below, which were also investigated with the cathodoluminescence microscope (Fig. 6).

Loseros tuff (Los)

The Loseros tuff is characterized by a distinctive laminated structure that shows a wide range of colors ranging from various shades of green, reddish brown, and lighter zones ranging from light gray, sometimes purple, and whitish (Fig. 4a). Both the greenish and reddish-brown laminations show distinct thin visible layers or bands. A multitude of dark lithic clasts (black to reddish-brown) and millimeter-sized phenocrysts are disseminated throughout the rock and are embedded in a fine-grained, ash-rich, and calcitic matrix. This felsic volcanoclastic rock is well-sorted and fine-grained. López-Doncel et al. (2013) distinguished two types, a fine-grained and a coarse-grained variety.

In thin section scans, the laminations associated with the reddish-brown layers are clearly visible under transmitted as well under polarized light. They are associated

**Table 3** Petrophysical properties of the investigated tuffs

ID	σ (vol%)	γ_b (g/cm³)	γ_m (g/cm³)	P_r (μm)	P_{mic} (%)	P_{cap} (%)	W_a (%)	S (−)	w (kg/m²√h) X	w (kg/m²√h) Z	μ (−) X	μ (−) Z	m_S (%)	α_{hy} (mm/m) X	α_{hy} (mm/m) X	α_{th} (10^{-6} K^{-1}) X	α_{th} (10^{-6} K^{-1}) Z	Salt (#)	TS (MPa) X	TS (MPa) Z	V_P (km/s) X	V_P (km/s) Z
Los	20.5	1.99	2.51	0.133	40	60	3.8	0.37	0.7	0.5	18.2	23.0	3.3	0.29	0.61	8.7	8.8	58	–	–	3.7	3.0
CR-Gto	19.1	1.90	2.35–	0.097	64	36	4.9	0.48	0.7	0.7	12.1	12.6	3.6	0.80	0.91	9.4	9.9	33	6.1	4.7	3.0	2.9
CHA	29.8	1.83	2.61	0.397	15	85	10.9	0.67	3.4	3.2	9.3	9.9	5.0	0.46	0.46	8.4	7.8	43	2.9	2.8	2.7	2.5
CHR	41.1	1.47	2.50	1.061	8	92	21.0	0.75	31.4	28.5	8.7	9.1	1.2	0.01	0.02	10.1	–	>83	2.5	2.1	2.3	2.2
ZaC	32.3	1.79	2.65	0.150	31	69	11.6	0.64	2.1	1.5	11.8	12.3	4.0	0.73	0.68	9.1	9.6	20	5.2	3.4	3.2	2.8
EIS	27.6	1.89	2.61	0.309	21	79	10.0	0.69	3.3	3.1	12.6	14.1	2.1	0.16	0.25	8.0	8.1	62	3.1	3.3	3.2	3.0
CV	28.3	1.71	2.39	0.114	35	65	13.2	0.80	1.9	1.7	14.0	13.9	3.4	1.29	1.16	8.8	9.3	25	4.0	3.6	2.9	2.4
PD n	28.9	1.82	2.56	0.365	14	86	12.0	0.75	9.7	5.0	14.8	14.2	2.7	0.02	0.04	10.4	9.5	>83	4.1	3.9	3.2	2.8
PD a	28.3	1.84	2.57	0.664	12	88	10.3	0.67	9.9	5.5	14.8	18.2	0.8	0.02	0.03	9.9	9.6	>83	4.5	4.3	3.2	3.0
TR	11.5	2.19	2.48	0.074	64	36	2.4	0.46	2.1	1.5	41.4	54.7	1.0	0.02	0.26	6.1	7.0	>83	8.1	7.4	4.4	4.3
RC	41.1	1.51	2.56	1.538	5	95	21.1	0.77	37.5	30.0	8.1	9.8	1.2	0.03	0.04	10.5	10.7	>83	2.7	2.0	2.4	1.9
ESC a	41.7	1.50	2.58	3.004	2	98	22.6	0.82	60.3	58.4	6.8	7.1	0.4	0.03	0.05	12.1	12.1	>83	2.1	1.8	2.2	2.0
ESC n	29.1	1.80	2.54	1.422	8	92	10.5	0.65	10.9	7.9	11.2	15.2	0.4	0.06	0.05	11.1	12.1	>83	–	–	3.3	3.0
CR ob	20.5	2.02	2.54	0.142	41	59	8.5	0.84	5.1	3.5	19	22	1.6	0.22	0.28	9.2	6.0	>83	5.0	4.1	3.1	2.9
CR-Mty	14.4	2.25	2.62	0.241	28	72	4.8	0.75	2.7	1.3	19.7	31.6	0.6	0.11	0.11	6.7	6.9	>83	–	–	3.3	3.3
BP	35.8	1.71	2.67	0.171	37	63	14.0	0.67	2.6	2.3	10.0	10.0	4.9	0.84	2.40	8.6	7.5	18	1.9	1.6	2.5	2.2
RSM	34.8	1.70	2.60	1.417	7	93	13.6	0.67	9.5	9.5	11.3	12.8	1.5	0.03	0.01	8.8	8.6	>83	5.2	5.0	3.2	3.0
CA	42.7	1.46	2.54	1.187	11	89	21.8	0.74	14.3	11.6	7.9	8.3	1.6	0.06	0.08	5.5	6.8	74	1.9	0.9	2.5	2.3
CG	55.9	1.08	2.44	4.073	4	96	41.4	0.80	78.4	62.2	6.0	8.1	1.2	0.01	0.20	5.4	3.1	>83	1.0	0.9	2.3	1.5
SG1	40.9	1.54	2.61	0.817	16	84	18.5	0.70	15.8	14.6	5.3	5.8	16.6	0.65	0.66	–	–	–	0.7	0.6	1.4	1.7
SG2	34.4	1.70	2.59	1.349	20	80	15.1	0.75	6.3	2.2	–	–	–	–	–	–	–	–	–	–	1.8	1.1
SG3	38.7	1.60	2.61	0.407	35	65	17.1	0.71	10.7	2.3	7.7	8.3	5.0	0.53	0.63	–	–	–	1.0	1.6	2.0	1.9
SG4	34.2	1.73	2.64	0.190	38	62	15.2	0.77	10.7	10.9	7.1	7.8	8.5	0.61	0.73	–	–	11	1.1	1.0	2.2	2.4
GF1	49.8	1.21	2.41	4.060	4	96	29.7	0.72	63.4	40.2	5.9	6.2	4.0	0.02	0.05	–	–	13	1.1	1.1	2.5	1.6
GF2	46.0	1.30	2.40	3.073	8	92	22.1	0.62	22.9	11.9	6.0	6.1	1.8	0.06	0.08	–	–	13	1.1	1.6	2.3	1.5
RG1	37.2	1.67	2.66	0.711	25	75	17.3	0.78	26.8	20.3	6.7	7.4	5.7	0.16	0.19	–	–	9	1.2	1.2	2.4	2.2
RG2	33.9	1.80	2.72	0.548	34	66	14.6	0.77	15.9	12.8	6.3	6.9	9.7	0.13	0.15	–	–	12	1.9	1.8	2.4	2.4
RG3	35.7	1.71	2.65	0.689	40	60	16.2	0.77	16.3	14.9	5.6	5.9	3.8	0.91	1.14	–	–	8	0.8	0.8	2.2	2.3
rTF	26.7	1.82	2.49	0.127	42	58	–	–	1.9	1.5	16.8	18.9	–	0.8	7.8	6.4	–	12	3.02	2.78	2.3	2.2
rTC	24.3	1.92	2.53	0.117	72	28	–	–	2.6	1.7	13.3	13.7	–	0.9	3.5	6.6	6.8	13	2.47	2.21	2.4	2.2
oLT	23.4	1.89	2.47	0.200	32	68	–	–	3.4	1.3	19.1	21.7	–	0.3	0.4	5.6	8.8	20	4.24	2.66	2.8	2.5
LC	11.1	2.27	2.55	0.089	79	21	–	0.84	–	0.8	83.9	87.3	–	0.4	1.0	6.4	7.9	>35	15.0	9.1	3.9	3.6
BJ	36.9	1.63	2.58	0.724	16	84	19.0	–	19.5	19.0	7.7	8.5	1.9	0.9	2.2	–	–	8	1.1	1.1	1.8	1.9
TLQ	28.0	1.67	2.32	0.097	53	47	–	–	3.5	3.1	–	–	–	0.3	0.9	11.3	11.6	6	1.9	1.8	2.5	2.5
PC	35.1	1.63	2.52	0.699	16	84	15.6	0.73	5.4	4.6	10.6	10.9	3.4	0.1	0.3	6.3	–	11	2.42	2.25	2.8	2.7
SU	40.0	1.55	2.59	0.980	6	94	18.2	0.71	14.9	13.2	9.5	9.9	0.9	0.04	0.6	–	10.8	>13	3.2	2.9	2.8	2.8
BE	26.8	1.88	2.58	0.365	23	77	9.7	0.68	3.4	2.2	10.3	11.5	2.6	0.4	1.6	6.7	7.2	12	2.9	2.7	2.8	2.8

Table 3 (continued)

ID	σ (vol%)	γ_b (g/cm³)	γ_m (g/cm³)	P_r (μm)	P_{mic} (%)	P_{cap} (%)	W_a (%)	S (−)	w (kg/m²√h) X	w (kg/m²√h) Z	μ (−) X	μ (−) Z	m_S (%)	α_{hy} (mm/m) X	α_{hy} (mm/m) Z	α_{th} (10^{-6} K^{-1}) X	α_{th} (10^{-6} K^{-1}) Z	Salt (#)	TS (MPa) X	TS (MPa) Z	V_P (km/s) X	V_P (km/s) Z
SC	38.1	1.62	2.62	0.740	14	86	20.0	0.85	19.1	13.1	8.9	8.6	1.7	0.1	0.4	–	–	7	1.4	1.1	1.9	2.0
FR	37.2	1.60	2.55	0.564	13	87	19.6	0.84	10.3	9.5	8.1	9.0	3.0	0.1	1.0	7.8	8.1	>13	2.7	2.4	2.5	2.5
oLK	24.7	1.90	2.53	0.261	38	62	–	–	1.9	1.6	12.1	12.2	–	1.2	1.7	2.8	3.3	8	–	–	2.3	2.1
wLK	36.6	1.43	2.25	0.508	19	81	–	–	–	–	–	–	–	–	–	–	–	–	–	–	–	–
TGQ	39.3	1.51	2.49	1.815	5	95	–	–	47.5	47.2	10.1	12.0	–	0.01	0.02	–	–	>20	3.58	2.97	2.4	2.3
TRC	24.6	1.95	2.59	0.407	15	85	–	–	0.5	0.4	25.9	27.0	–	–	0.03	–	–	>20	7.87	6.53	3.5	3.3
TQG	13.3	2.00	2.31	0.039	69	31	–	–	0.5	0.9	–	–	–	–	–	–	–	>20	–	–	3.2	3.0
TRH	37.6	1.60	2.57	1.163	8	92	–	–	27.5	22.5	10.6	14.7	–	0.08	0.12	–	–	>20	3.52	2.94	2.3	1.9
TAH	44.0	1.45	2.58	1.191	8	92	–	–	34.8	25.6	8.2	9.9	–	0.13	0.19	–	–	16	1.7	1.56	1.7	1.4
WT	58.4	0.91	2.19	1.101	19	81	–	–	46.3	42.4	–	–	–	0.26	0.45	–	–	7	–	–	2.0	1.6
BT	46.2	1.35	2.51	0.542	26	74	–	–	23.3	19.2	13.0	13.2	–	0.12	0.29	–	–	12	2.6	2.0	2.6	2.3
LPW	18.9	2.02	2.49	0.487	20	80	–	–	1.6	1.5	–	37.5	–	0.05	0.12	–	–	>20	5.1	4.9	3.3	3.3
TDW	25.3	1.96	2.62	–	–	–	–	–	1.6	–	–	–	–	–	–	–	–	>20	–	–	3.5	3.2
LPR	13.3	2.24	2.58	–	–	–	–	–	1.2	1.5	–	–	–	–	–	–	–	8	–	–	2.9	2.7
TGA	39.4	1.5	2.48	1.972	5	95	22.6	0.24	41.6	24.6	89.0	–	–	0.06	0.10	–	–	>20	–	–	2.2	2.2
CH	8.0	2.37	2.58	0.358	27	73	–	–	0.4	0.4	118.6	–	–	0.29	0.30	–	–	>20	5.1	5.6	2.2	–

ID sample ID, σ effective porosity, γ_b bulk density, γ_m matrix density, P_r pore radius, P_{mic} micropores, P_{cap} capillary pores, W_a water absorption, S saturation coefficient, w capillary water uptake, μ water vapor diffusion resistance coefficient, m_s hygroscopic sorption at 95% RH, α_{hy} hydric expansion, α_{th} thermal expansion coefficient, *TS* tensile strength, V_P ultrasonic velocity

[a]From Wedekind et al. (2013)
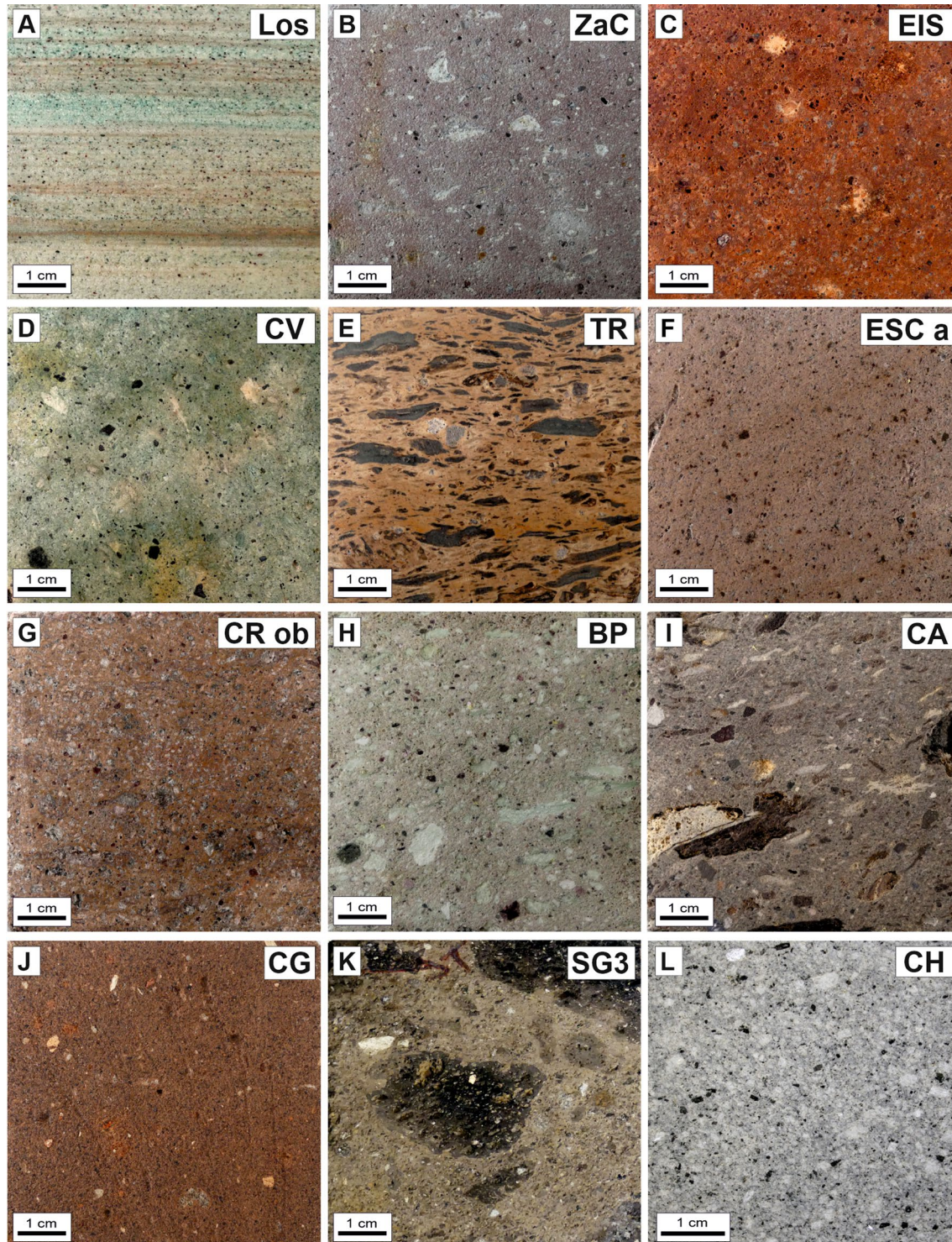
with very fine-grained ash-rich layers, which are essentially opaque zones under polarized light. The main mineral constituents are quartz, K-feldspar, plagioclase, and calcite. Quartz occurs as angular crystals, whereas both feldspars are angular to subhedral. Minor biotite shows a greenish color in transmitted light and considerable alteration. Close examination of the rock reveals that the groundmass is made up of extremely fine-grained crystallites and a low amount of remaining glass shards, and thus, the fabric can be considered to be hypocrystalline to holohyaline. Based on the system of Schmid (1981), the Loseros tuff can be classified as a lithic tuff or as an ash tuff according to Fisher (1966).

◄**Fig. 4** Macroscopic fabrics in the selected tuffs of the study. **a** Loseros tuff (Los): well-sorted volcanoclastic rock showing distinct laminations, and also containing dark lithic fragments. **b** Light pink Zacatecas tuff (ZaC) containing collapsed pumice clasts. **c** Bright reddish orange El Salto tuff (EIS) rich in crystals and lithoclasts. **d** Massive Cantera Verde tuff (CV) showing a mottled greenish color and considerable lithoclasts. **e** Toba Rosa (TR) ignimbrite containing extremely flattened vesicular clasts oriented parallel to the flow direction. **f** Light reddish brown Escolasticas tuff (ESC a) that contains numerous small lithoclasts. **g** Massive Cantera Rosa Obscura tuff (CR ob) that contains lithoclasts and visible feldspar phenocrysts. **h** Blanca Pachuca (BP) tuff with numerous weathered pumice clasts. **i** Cantera Amarilla tuff (CA) containing large, flattened scoria and pumice clasts also aligned to the flow direction. **j** Highly porous and low density brownish Cantera Gris tuff (CG), which contains occasional lithoclasts. **k** Brownish Gris Oscura tuff (SG3) containing large dark gray scoria clasts. **l** Grayish Chiluca tuff (CH) showing large plagioclase phenocrysts and hornblende crystals (image from Wedekind et al. 2011)

Under the cathodoluminescence microscope the presence of calcite shows a reddish-orange color and occurs as grains similar in size to the fine-grained quartz and feldspars, but also in very fine grain sizes (Fig. 6a). Calcite shows no zoning, but does show different zones of luminescence (possibly two generations) and at the grain contacts evidence for later dissolution. Calcite makes up around 10 percent of the rock. Ranges of 5–20% calcite have been reported by Wedekind et al. (2013).

Altered feldspars show a greenish color, whereas the unaltered grains similar to quartz, show almost no luminescence. The ash-rich matrix shows no luminescence and only at longer exposure times does quartz begin to show a dark violet CL color.

Zacatecas Cathedral (ZaC)

The Zacatecas Cathedral tuff is a fine-grained, light pink tuff that also shows an iron oxidation staining or localized mottled areas due to the oxidation of Fe-rich lithoclasts (Fig. 4b). Embedded in the fine-grain matrix are lithoclasts comprising collapsed vesicular pumice and scoriaceous lava fragments with color variations consisting of white, gray, and reddish-brown. Where the lithoclasts have weathered out, the surface of the rock appears porous.

Overall, the fabric of the Zacatecas tuff is glassy, which under the microscope is essentially opaque except where devitrification of the glassy material forms evenly distributed very fine-grained crystallites. Collapsed pumice fragments are also opaque under polarized light. Around 5% of the rock contains fine-grained fractured quartz crystals, which are anhedral to subhedral and minor K-feldspar. Under the microscope the dark reddish-brown lava fragments are almost opaque and show alteration to extremely fine-grained, possibly clay minerals that show a higher birefringence. Trace amounts of gypsum were identified by the XRD analyses in this study and were also identified in the thin section as a very fine-grained euhedral crystal. The composition of this tuff with its sizeable percentage of pumice and glass allows it to be classified according to Schmid (1981) as a vitric tuff and by the system of Fisher (1966) as a lapilli tuff.

Under the CL microscope, the shard-like structure of the > 90% glassy matrix becomes visible; however, it has a low luminescence where the devitrified parts show a dark violet color and the relict shards a dark brown color. The fractured quartz crystals show a bluish-violet color but no zoning. CL also revealed a fine-grained anhedral crystal showing a reddish luminescence suggestive of calcite. Scattered throughout the groundmass are microscopic specks that show an orange-red to yellow color, suggesting either calcite or apatite. However, the XRD analyses did not detect these minerals.

El Salto (EIS)

The tuff known by the trade name El Salto is a porous, bright reddish orange rock, rich in millimeter-sized crystals and lithoclasts (Fig. 4c). The lithoclasts are gray, dark reddish-brown to yellowish-white. The yellowish-white lithoclasts (altered pumice?) range in size from < 2 mm up to 1 cm. Quartz and feldspar crystals can be identified in hand specimens. Both crystals and lithoclasts are also distributed homogeneously throughout the rock, as well as the visible pore spaces.

The fabric of this tuff can be described as being hypocrystalline, where the 10% volume of crystals are supported by the devitrified glassy matrix. The crystals are mainly composed of anhedral quartz, with a trace amount attributed to cristobalite/tridymite according to the XRD investigation, and anhedral to euhedral K-feldspar also occurring as laths. Furthermore, the XRD investigation also identified smectite occurring as a major component in the groundmass. Most of the crystals are fractured to shattered. The glassy matrix also seems to have undergone considerable devitrification. With the high glass content, the El Salto tuff classifies according to Schmid (1981) as a vitric tuff and as a lapilli-ash tuff using Fisher (1966).

The CL investigation has provided considerable insight (qualitatively) into the mineralogical composition of the El Salto tuff. The K-feldspar crystals show excellent luminescence with its typical blue color. Lithic fragments show no luminescence; however, they do exhibit abundant extremely fine-grained inclusions similar to calcite luminescence. K-feldspar crystallization has also taken place around some of the lithic clasts. The very fine-grained groundmass dominates with a quartz composition exhibiting a dark reddish purple color with a lower luminescence.
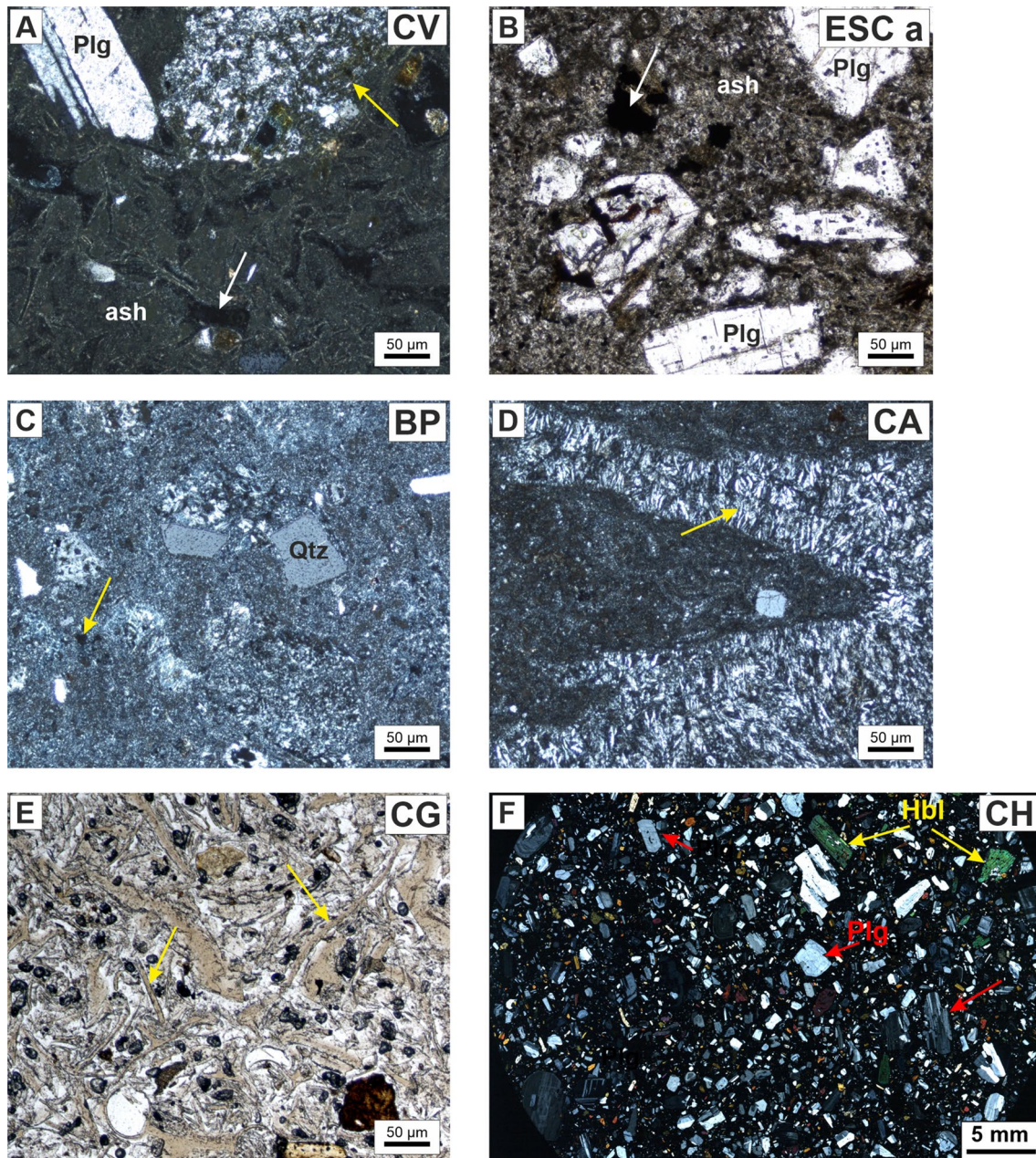
Fig. 5 Thin section fabrics of the selected tuffs. **a** Cantera Verde Oaxaca (CV) is a vitric ash tuff. Glass shards (white arrow) show extremely fine-grained microlites along the shard rims. The ash-rich matrix is also opaque. Plagioclase (Plg) occurs as twinned phenocrysts. Lithic fragments are indicated by the yellow arrow. Image under plane polarized light. **b** Escolasticas (ESC) tuff under transmitted light showing a very fine-grained altered ash-rich matrix. Plagioclase occurs as laths or as angular crystals. Opaques are also visible (white arrow). **c** Blanca Pachuca (BP) under plane polarized light shows a strong cryptocrystalline ash-rich matrix. Quartz (Qtz) along with K-feldspar occur as anhedral crystals. Opaques are also vis-

ible (yellow arrow). **d** Unique microstructure visible in the Cantera Amarilla (CA) tuff. Pumice clast with a fine-grained cryptocrystalline ash-rich matrix core with perpendicular "feather-like" crystal growth at the rims (yellow arrow). **e** Characteristic glass shard fabric in the Cantera Gris (CG) tuff in transmitted light. Glass shards indicated by the yellow arrows. **f** Thin section scan of the Chiluca tuff (CH) depicting the crystal-rich fabric. Plagioclase (Plg) occurs as twinned and zoned phenocrysts (red arrows). Hornblende (Hbl) also occurs as phenocrysts (yellow arrows) as a minor component throughout the fabric
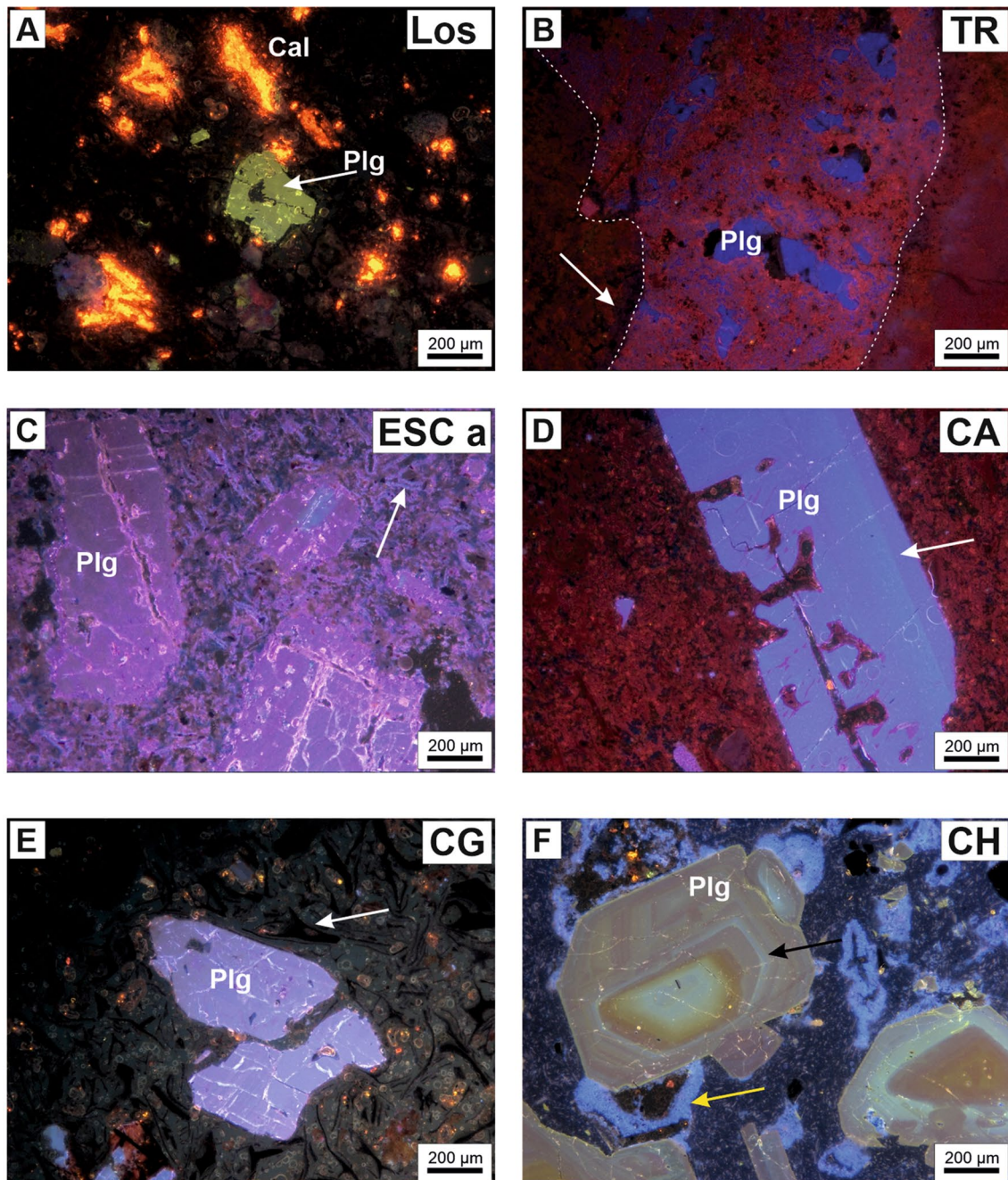
Fig. 6 Characteristic cathodoluminescence fabrics and microstructures in the selected tuffs of the study. **a** Visible calcite (Cal) mineralization oriented parallel to the main lamination in the Loseros tuff. Altered plagioclase (Plg) appears green under CL. Ash-rich matrix shows no luminescence. **b** Quartz-rich, very fine-grained matrix in the Toba Rosa ignimbrite shows a reddish to violet luminescence. Coarse anhedral plagioclase grains (Plg, blue luminescence) occur in the flattened clasts (outlined by dashed lines). Low to non-luminescent areas are vitric rich areas in the fabric (white arrow). **c** Fractured phenocrysts of plagioclase in the Escolasticas tuff show a purple luminescence and occasional blue cores. Relict glass shards are also visible by the luminescent bluish microlites outlining the rims (white arrow). Non-luminescent areas are very fine-grained ash-rich areas.

d Zoned bluish plagioclase phenocryst in the Cantera Amarilla tuff embedded in a quartz-rich ash groundmass (white arrow). Non-luminescent areas in the fine-grained matrix is glass. **e** Well-preserved glass shards (non-luminescent) are easily identifiable in the Cantera Gris tuff (white arrow). These are embedded in a low luminescent cryptocrystalline ash matrix. Minor plagioclase, broken and fractured shows a bluish to violet color and indications of zoning is discernible. **f** Distinctly zoned plagioclase phenocrysts in the Chiluca tuff. Low luminescent microlite laths of plagioclase (violet) are visible in the non-luminescent ash-rich matrix. The bright bluish areas (yellow arrow) in the ash matrix correlate to very fine-grained cloudy zones suggestive of the mineral kaolinite

Also occurring in the groundmass and evident by CL, is a coating by smectite (showing a blue color) in the quartz-rich groundmass.

Cantera Verde (CV)

Cantera Verde tuff is a massive rock that shows various shades of green from light to dark giving the altered rock a somewhat mottled appearance. The tuff contains considerable clasts containing very dark volcanic rock fragments and, in some cases, altered and flattened pumice clasts also showing a greenish coloration (Fig. 4d). The clasts range in size from less than a few mm to greater than 1 cm. Cantera Verde tuff can be classified as a vitric ash tuff or a lapilli tuff using the systems of Schmid (1981) and Fisher (1966).

Overall, the fabric of this rock can be considered an ash-rich hypocrystalline tuff with approximately 7% of the crystals supported by the groundmass. In thin section, the ash-rich fabric is essentially opaque. Under transmitted light the shard structures are visible, where individual shards are outlined by micro-crystallites representing the process of devitrification (Fig. 5a). The main mineral constituents are quartz, plagioclase, and the zeolite mineral clinoptilolite (determined by XRD analysis). This is followed by K-feldspar and traces of muscovite/illite. A 0.1 mm altered muscovite flake was observed in the thin section. Many of the lithic fragments are almost opaque in polarized light, except for the very fine-grained crystal inclusions of twinned plagioclase. Feldspars are subhedral to euhedral and quartz anhedral. The crystals are in part fractured and show no discernible orientation.

Under the CL microscope, the lithic fragments show blue colors typical of feldspar. They contain subhedral to euhedral inclusions that exhibit two distinct CL colors: a low luminescent brownish color to bright orange. These are interpreted to be simple zoned crystals of quartz. The ash-rich groundmass shows essentially no luminescence. Fractured plagioclases show zonations with CL colors defined by violet to a bluish core. CL also reveals that some of the shards show a low luminescent blue colored outline. Also present are strongly luminescent yellowish crystals (apatite?), partially zoned that are associated with the blue colored K-feldspars.

Toba Rosa (TR)

Toba Rosa is a light brown to tan colored ignimbrite, where the less weathered zones appear more whitish in color. The fine-grained matrix predominantly contains grayish, vesicular, and extremely flattened volcanic rock fragments with a distinct orientation (Fig. 4e). This represents the flow direction of the pyroclastic material. Some of the lithoclasts are rounded to subrounded. These scoriaceous clasts also

contain smaller clasts of gray, whitish and reddish volcanic fragments. Using the classification system of Schmid (1981) and Fisher (1966), the Toba Rosa tuff can be assigned to a vitric ash tuff or a lapilli tuff ignimbrite, respectively.

In complete thin section scans, a very fine micro-layering is observable in the ash-rich matrix. The large flattened volcanic clasts are also aligned to this layering. The dominant phase is quartz in the fine-grained ash-rich matrix followed by plagioclase and K-feldspar, which are subhedral to euhedral and fractured. Both the euhedral quartz and feldspar phenocrysts also show alignment to the main rock fabric. The flattened volcanic clasts show crystal growth perpendicular to the axis of the main layering. XRD analyses indicate that kaolinite occurs as a minor component and hematite as a trace constituent.

Under the CL microscope the K-feldspars and plagioclase exhibit the typical blue color, but no zonations are observable. Their luminescence is low to medium. The fine-grained ash matrix consists predominantly of quartz and shows a strong reddish-violet color, along with very fine-grained feldspars showing a dark blue CL (Fig. 6b). However, some of the bluish color may be the result of the presence of kaolinite. Coarse sand-sized lithic clasts (occurring as angular fragments 2–4 mm in size) consist of quartz and feldspar and show a slightly higher CL intensity. Other clasts essentially showing no luminescence host very fine-grained inclusions exhibiting orange (calcite?) and bright green CL colors (apatite?).

Escolasticas (ESC a)

Escolasticas is a fine-grained, porous, light reddish brown tuff (weathered sample) with numerous gray and dark reddish brown millimeter-sized lithoclasts (Fig. 4f). Phenocrysts > 1 mm in size are also visible in hand specimens. Using the Schmid (1981) and Fisher (1966) classification system, the Escolasticas stone can be classified as a vitric tuff with a hypocrystalline fabric and as a lapilli ash tuff.

Complete thin section scans show that the rock contains a crystal volume of around 30%, where plagioclase and according to XRD analyses, cristobalite/tridymite are the dominant phases. The plagioclase crystals also show a rudimentary alignment as indicated by plagioclase laths showing a similar orientation. Many of the crystals are cracked to fragmented (Fig. 5b). The fine-grained ash-rich matrix is almost opaque.

Plagioclase occurs as anhedral, subhedral, and euhedral crystals showing the characteristic polysynthetic twinning. XRD analyses indicate that quartz, hornblende and hematite occur as trace phases. Cristobalite/tridymite was not identified in the thin section, but probably occurs along with feldspar as a component making up the ash-rich groundmass (Fig. 5b).

Under the CL microscope, the plagioclase phenocrysts show rudimentary zoning, where the core of the crystal shows a bluish color and transitioning to a more reddish violet color towards the rim. CL also makes visible a relict shard fabric, where the shard cores are non-luminescent and rimmed with a bluish color (feldspar?) (Fig. 6c). Also observed are unknown crystals showing a yellow CL color associated with dark opaque lithic clasts. Moreover, inclusions of an unknown elongated subhedral crystal are observed in a plagioclase exhibiting a yellowish and a reddish brown CL color.

Cantera Rosa Obscura (CR ob)

The massive Cantera Rosa Obscura tuff is a light to medium reddish brown pyroclastic rock with white, dark red and a few grayish lithoclasts. Feldspar phenocrysts can also be seen macroscopically (Fig. 4g).

The rock has a hypocrystalline fabric, where 45% of the unoriented feldspar crystals are supported in an ash-rich groundmass. Dominant phases are plagioclase, quartz, and according to the XRD analyses kaolinite also contributes as a major mineral phase. K-feldspar and cristobalite/tridymite are major phases with hematite and muscovite/illite occurring as trace components. K-feldspar shows a wide range of shapes from angular, slightly rounded to subhedral and forms the large crystals in the rock fabric. Plagioclase occurs as laths and angular fragments and shows simple twins. The crystals also show little fracturing.

Cathodoluminescence reveals a complex fabric especially in the ash-rich groundmass. K-feldspar and plagioclase show two different CL colors. Plagioclase tends to a violet color, whereas K-feldspar shows a blue color. Faint zonations are visible in both crystals. Much of the ash-rich groundmass shows a very low luminescence, except where specific lithic fragments are outlined by a bluish CL color. Given the high concentration of kaolinite detected by XRD analysis, this may represent where this clay mineral is localized in the rock fabric. Based on the above characteristics and the classification systems of Schmid (1981) and Fisher (1966), Cantera Rosa Obscura can be classified as a vitric ash tuff.

Blanca Pachuca (BP)

Blanca Pachuca is a very fine-grained, light grayish tuff with dark gray lithic fragments and occasional medium to dark red vesicular cinder clasts. Moreover, strongly weathered pumice ranging from a few mm to > 1 cm in size occur as flattened, subrounded and angular clasts. All these volcanic fragments are embedded in a very fine-grained ash-rich matrix (Fig. 4h). Note: XRD did not detect any zeolites.

Utilizing the system of Schmid (1981) and Fisher (1966) this tuff can be classified as a crystalline ash tuff.

The dominant phases in this tuff are plagioclase, quartz, and mixed layer clay minerals according to the XRD investigation. The ash matrix is cryptocrystalline (Fig. 5c). Minor K-feldspar and minor quartz occur as anhedral to subhedral crystals > 1 mm in size. The fabric is dominated by the different clasts and the cryptocrystalline matrix. No distinct orientation of the clasts is recognizable, except that the overall fabric also appears somewhat brecciated.

Under the cathodoluminescence microscope, the Blanca Pachuca tuff shows a low luminescence in essentially the cryptocrystalline ash matrix, in the lithic fragments and even in the feldspar and quartz crystals. Longer exposure times with the digital camera do reveal that quartz exhibits a somewhat orange color and plagioclase a dark bluish violet color. Indications of very fine-grained bluish K-feldspar inclusions are found in some clasts. Also observable in some clasts are crystals showing no luminescence (glass?) associated with quartz and feldspar.

Cantera Amarilla (CA)

The Cantera Amarilla tuff is a light to medium gray tuff with a large variety of different types of volcanic lithoclasts (Fig. 4i). Lithoclasts include mm to cm sized gray vesicular scoria, coarse dark gray volcanic fragments, reddish brown cinder and porous light yellowish brown flattened and elongated pumice fragments aligned to the flow direction. This rock has been classified as a vitric lapilli tuff according to the system of Schmid (1981) and Fisher (1966).

Quartz, plagioclase, and glass are the dominant phases along with K-feldspar. XRD analyses detected mixed-layer clays as a trace component. In thin section some of the pumice clasts show a unique crystallization fabric where the cores exhibit an apparent randomly oriented cryptocrystalline structure and at the rims, a fine-grained feathery-like crystal growth perpendicular to the core and the groundmass (Fig. 5d). The groundmass surrounding these clasts exhibits a relict shard fabric, where the shards also show alteration and very fine-grained crystal growth perpendicular to the shard rim. Phenocrysts of subhedral to euhedral plagioclase make up about 2% of the rock. Glass, which shows no devitrification, is opaque.

The CL investigation shows that the pumice clasts with the distinct crystal growth structures show a low luminescent reddish color, but in some crystals a brighter reddish core is visible and are interpreted as quartz rich clasts. Shards that are unaltered show no luminescence. The feldspar phenocrysts are zoned and exhibit a bluish CL color (Fig. 6d).

Cantera Gris (CG)

The Cantera Gris tuff is a brown, highly porous rock of low density. Occasional inclusions of light reddish brown weathered cinder, black pumice, light gray vesicular scoria and weathered yellowish white pumice occur ranging in size from < 1 mm to around 1 cm (Fig. 4j). Based on the composition and components in this rock, the Cantera Gris can be classified as a vitric ash tuff.

In thin section, the dominant phases identified are quartz occurring as the cryptocrystalline ash matrix, followed by the characteristic shards of broken gas bubble walls (most distinct in this specimen, Fig. 5e), and minor anhedral to subhedral K-feldspar present as phenocrysts. Very few crystals of anhedral and euhedral twinned plagioclase were also identified, which are also slightly deformed. Mixed layer clays were detected as a major component by XRD. Traces of gypsum and hematite were also identified by this method.

Under the CL microscope, the morphology of the broken shards is easily identifiable. They are non-luminescent (black) and embedded in a low luminescent cryptocrystalline quartz matrix (Fig. 6e). The crystals of plagioclase show a bluish CL color and indications of zoning could be detected. Possible gypsum (?) or apatite showing bright CL colors are visible in the matrix and in some of the volcanic clasts.

Gris Oscura tuff (SG3)

The Gris Oscura is a brownish-gray tuff with a grain size ranging from 0.2 to 0.5 mm. Large dark gray scoriaceous clasts distinguish this tuff (Fig. 4k). They are angular to subrounded and also contain fine-grained inclusions. Utilizing the systems of Schmid (1981) and Fisher (1966), the Gris Oscura Tuff can be classified as a vitric crystal tuff showing a hypocrystalline fabric.

The defining character of this tuff is the sizeable percentage of crystals, especially phenocrysts of plagioclase embedded in a very fine-grained ash-rich vitric groundmass (brown in transmitted light). The plagioclase crystals range in size from < 1 mm up to > 5 mm and are anhedral to euhedral. Some phenocrysts are twinned, strongly fractured, and broken, and in some larger crystals zoning is evident. Where the plagioclase phenocrysts are highly fractured, alteration in these areas is evident. No orientation is evident for the crystal components. Opaques are scattered throughout as larger grains (black lithic fragments?) and also occur as finer particles in the ash-rich glassy matrix.

The ash-rich glassy matrix is non-luminescent under CL. Plagioclase shows zonations where the colors range from bluish to violet and greenish. A few plagioclase crystals almost show a complete green color, indicative of alteration. Minor K-feldspar is evident by crystals showing a strong blue CL color. Periodically in the non-luminescent glassy groundmass, very fine-grained and in some cases euhedral crystals occur. These show an orange-red color and darker cores, and are interpreted as being quartz.

Chiluca (CH)

Chiluca is a gray tuff containing mafic and felsic lithoclasts (see Wedekind et al. 2011). Both the coarse feldspar and hornblende give the rock a porphyritic appearance (Fig. 4l).

Chiluca tuff is in some respects similar to the Gris Obscura in that both have a large volume of plagioclase crystals embedded in an ash-rich glassy hypocrystalline fabric (Fig. 5f). The difference is the presence of hornblende and minor biotite and that the glassy matrix is light gray. Plagioclase is the dominant mineral phase and is subhedral to euhedral. It is zoned, shows the characteristic twinning, and many of the large phenocrysts (> 4 mm in size) are strongly fractured or broken. Strong alteration of these crystals occurs in the core and at the rims. No crystal orientation or flow textures are evident.

Hornblende is present as a minor phase and is oriented in both the 110 and 011 planes. In transmitted light some of the hornblendes show indications of zoning in the 110 plane. Some of the hornblendes contain inclusions of quartz or apatite.

In polarized light most of the ash-rich glassy matrix appears opaque. However, very fine-grained crystals showing a lath-like morphology are observable and are interpreted to be micro-crystallites of feldspar.

The best example of zoning under the CL microscope can be found in the Chiluca tuff (Fig. 6f). Plagioclase exhibits elaborate growth zonations with colors ranging from violet to yellowish green, which is suggestive of the trace elements Fe^{3+}, Fe^{2+}, Ti and Mg. Hornblende shows no luminescence, however, the inclusions (some may be euhedral) show light to medium orange CL colors (probably zonations). These are not only limited to the hornblende crystals, but can also be found in the matrix or some feldspar crystals.

The ash-rich glassy matrix shows a low luminescence, whereas the very fine-grained crystallite laths also show a similar luminescence to the plagioclase crystals. Most distinct in this tuff are the strongly bluish luminescent zones that occur through the matrix in contact with the main mineralogical phases. The color is similar to K-feldspar, however, in polarized light these zones appear as extremely fine-grain cloudy zones suggestive of perhaps the clay mineral kaolinite.

The tuffs in this study were also classified according to the system of Schmidt (1981) and Fisher (1966). Most of the

tuffs investigated classify as vitric tuffs, followed by crystal tuffs, and two were found to be lithic tuffs (Fig. 7a). Using the system of Fisher (1966), the tuffs are classified as lapilli and ash tuffs (Fig. 7b).

Geochemically, the 32 of the volcanic tuffs investigated in this study can be classified as acid rhyolites, dacites, or trachytes/trachydacites and andesites. These are plotted in the total alkali silica diagram (TAS) in Fig. 8. The samples are also indicated by their classification into lithic, vitric, and crystal tuffs. Two lithic tuffs plot as dacites, whereas the crystal tuffs plot in three fields as andesites, dacites and rhyolites as a result of compositional differences. The majority of the vitric tuffs are found in the rhyolite field.

Clay mineralogy

The clay mineral composition of 28 tuffs was determined by X-ray diffraction (XRD) (Table 2; Fig. 9). All the tuffs investigated are mainly composed of quartz and/or cristobalite/tridymite followed by feldspar (K-feldspar, plagioclase). Only two tuffs studied by XRD are free of feldspar (rTC, TLQ). In most tuffs, hematite is present in trace amounts. Some tuffs are dominated by a mineral (or rich in a mineral) that is only present in these particular tuffs: clinoptilolite (CV), alunite (TLQ), or in a few tuffs only: calcite (Los, CR-Gto, CA). A glassy matrix was evident by XRD only in CG. Some tuffs only contain trace phases present in a few tuffs, e.g., hornblende (ESC a, ESC n), diopside (CHR), anatase (CHA), or gypsum (ZaC). Clay mineral analysis of fractions < 2 μm was performed in most tuffs except in the following samples: CHR, CV, ESC a, and ESC n. In all fractions < 2 μm expandable clay minerals were present in different amounts. Twelve tuffs contain large amounts of kaolinite (in one case possibly kaolinite or halloysite). Traces of muscovite/illite are present in 13 tuffs and in only one tuff, oLK, is the stone dominated by muscovite/illite.

XRD and CEC results of the swellable clay mineral content

The most interesting aspect regarding damages due to hydration is the presence of expandable clay minerals that allow intracrystalline swelling with water. Such phases were determined in all tuffs where clay fractions were analyzed; and in CR-Gto. Cantera Verde, however, contains a zeolite instead of expandable clay minerals. Expandable clay minerals have a shared feature being the interlayer region where exchangeable cations can be readily exchanged by competing cations, and these cations can be hydrated and dehydrated easily. A proxy for expandable clay minerals (Ruedrich et al. 2011) is the cation exchange capacity (CEC), which can be analyzed by an extraction method (here Cu-triethylenetetramine was used). The second column in Table 2 indicates if the CEC can be explained by the clay mineralogy analyzed. In most cases this can be confirmed immediately. In a few samples, the CEC is lower than expected from a mineral analysis of the clay fraction < 2 μm by XRD (Fig. 8). In these samples with a low CEC the total amount of clay fraction is unknown: EIS, PD n, BP, CA, and BJ. The sample with the highest CEC of 25 meq/100 g is CR-Gto, containing approximately 25 mass% smectite or smectitic (= expandable) interlayers, which is a very large amount for a natural building stone. This sample has a saturation coefficient of 0.48 indicating weathering and frost resistance. Again, this is a good example that not only the amounts of expandable clay minerals are important but their position in the matrix. If such expandable clay minerals are located in open pores of a tuff rock, they can expand without building up a significant
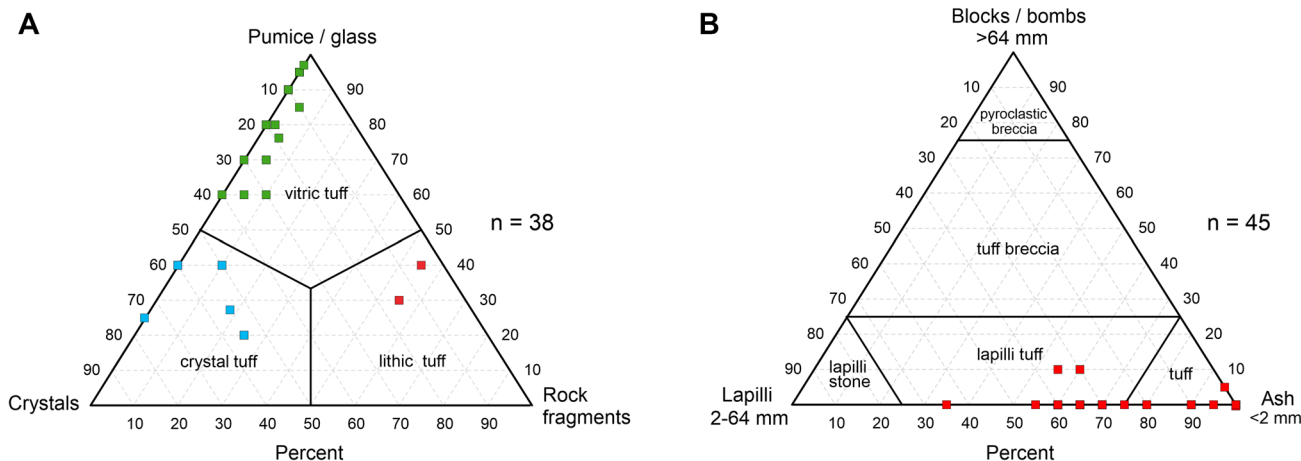
Fig. 7 Classification of the tuffs. **a** Based on Schmidt (1981) the tuffs can be classified into vitric, crystal and lithic tuffs. **b** Using the system of Fisher (1966), the tuffs classify as lapilli and ash tuffs. Many of the samples plotted have the same volume percent, e.g., 17 tuffs in the Fisher system are 100% ash tuffs

Fig. 8 Geochemical classification according to the total alkali–silica diagram after Le Bas et al. (1986). The tuffs are indicated by their pyroclastic content based on the classification system of Schmidt (1981): red = lithic tuff, blue = crystal tuff, green = vitric tuff
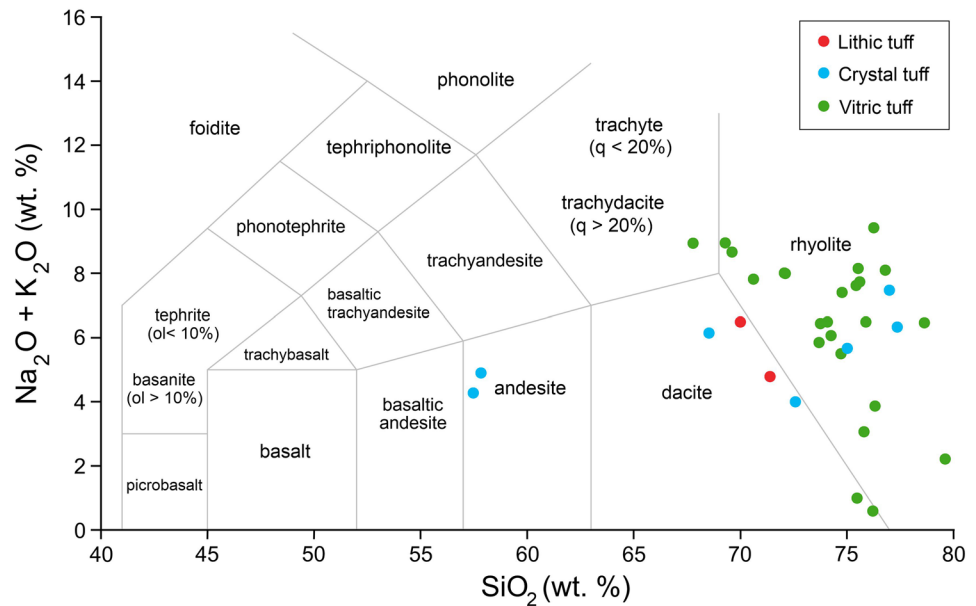
Petrophysical properties

Determining the petrophysical properties of natural stones is a prerequisite to assessing the quality of a building stone. Given the great diversity of the Mexican tuffs (their heterogeneity, origin, composition, fabric, groundmass, etc.), 53 samples were collected to investigate their petrophysical properties. The data compiled in this study are listed in Table 3.

Pore space properties

The investigated tuffs are mainly characterized as highly porous, with porosities ranging from 8.0 to 58.4 vol% and a median porosity of 34.2 vol%. Despite the wide range from 0.91 to 2.37 g/cm^3, the respective bulk densities are accordingly low, with a median of 1.71 g/cm^3. Fairly low porosities are shown by the tuffs Chiluca (CH), La Cueva (LC), Toba Rosa (TR), Amarilla de la Cañada Marqués (TAC) and Cantera Rosa Monterrey (CR-Mty), with values between 8.0 and 14.4 vol%. The highest porosities are reached by the gray tuffs of San Miguel de Allende (GF1, GF2, CG) and the white and black tuffs from Queretaro (WT, BT), which obtain extreme values of 46.0–58.4 vol%.

The low porous tuffs are usually characterized by a small mean pore radius (down to 0.039 μm for TAC) and hence an increased fraction of micropores (69% for TAC). The highly porous tuffs obtain mean pore radii that are partly more than a hundred times bigger (up to 4.073 μm for CGa) and accordingly high fractions of capillary pores (96% for

CGa). From 51 out of the 53 tuffs of the dataset (Table 3), the pore throat radii were investigated. Their median pore radius amounts to 0.542 μm. The median tuff of the data set obtains a fraction of 20% micropores and 80% capillary pores. The distribution of the pore throat radii can be classified according to Ruedrich and Siegesmund (2006) as unimodal equal (type I), unimodal unequal (type II) or bimodal (type III). The majority of the Mexican tuffs show a variable distribution of pore throat radii. Pore radii distributions are shown for the samples CG, CV, GF2 and RG1 (Fig. 10).

Water absorption, transport and retention

With such high median fractions of capillary pores (~ 80%), the respective total water absorption and capillary water absorption values are highly increased for the median Mexican tuff. Sorption curves for the tuffs Los, CR, CV and RSM are shown in Fig. 11. The total water absorption capacity upon immersion under forced (vacuum) conditions ranges between 4.9 and an incredible 63.9 wt%. The median tuff in this data set has the capacity to absorb 20.0 wt% under forced conditions. Since the total water absorption under voluntary (atmospheric) conditions, which was investigated for 35 tuffs (with a median of 20.9 wt% for forced water absorption), is almost 6 wt% lower (median of 15.2%), the respective saturation coefficients amount to 0.74. The dimensionless saturation coefficient *S* describes the amount of pore space that is accessible to water and gives an estimation of the material's weathering and frost resistance, by dividing the total water absorption under vacuum conditions by the water absorption under atmospheric conditions (Hirschwald 1912). Values under 0.75 indicate weathering and frost resistance, while the frost resistance remains uncertain between 0.75
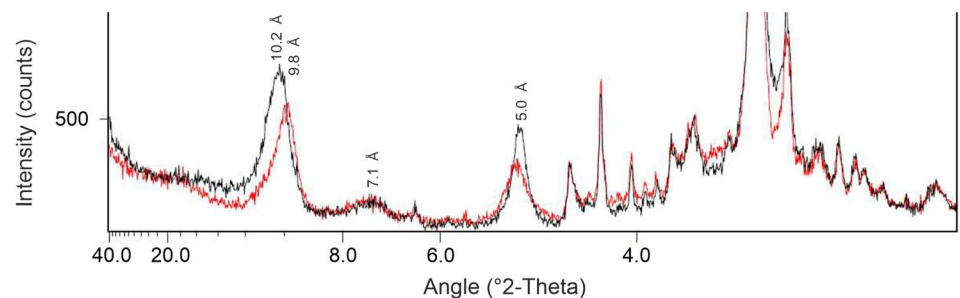
Fig. 9 Examples of expandable clay minerals in tuffs as analyzed by XRD. The shared property is the expandable interlayer region reacting with peak shifts upon solvation with ethylene glycol (red lines) compared to air-dry state (black lines). **a** PD n (only smectite), **b** Los (interstratified illite–smectite phases with a low degree of ordering), and **c** BP (interstratified illite–smectite with a high degree of ordering)
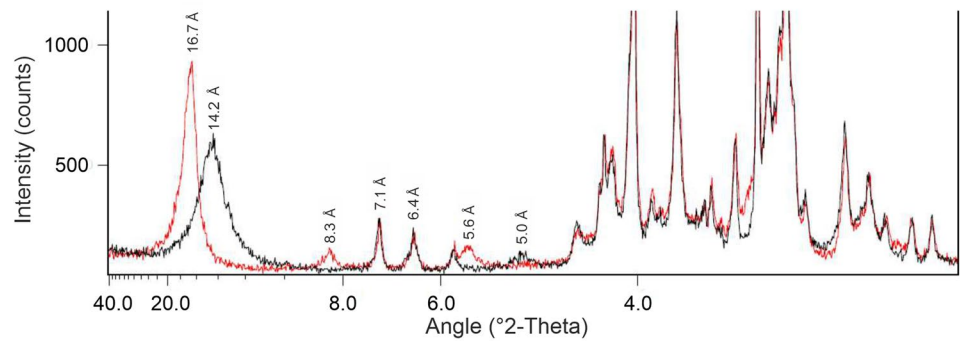
Sample PD n, CEC = 4 meq/100 g; expandable clay minerals: smectite without an interstratified component.
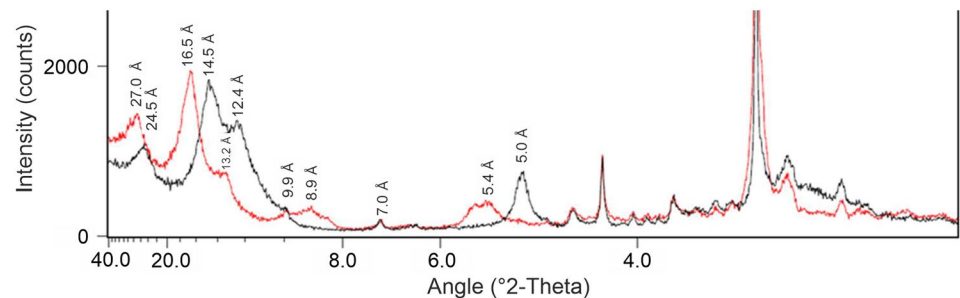
Sample Los, CEC = 18 meq/100 g; expandable clay minerals: two types of interstratified illite-smectite with low degree of ordering.

Sample BP, CEC = 5 meq/100 g; expandable clay minerals: interstratified illite-smectite with high degree of ordering.

and 0.9, and values over 0.9 indicate a lack of frost resistance. With an S value of 0.74, the median Mexican tuff of this data set is therefore classified as barely frost resistant. It is striking that tuffs with a larger mean pore throat radius tend to obtain higher S values (Table 3).

The capillary water absorption (w value) varies widely, from barely anything (0.4 kg/m$^2\sqrt{}$h for CH and TRC) to extremely high values of 78.4 kg/m$^2\sqrt{}$h (CGa). The highest potential for capillary water absorption is achieved by highly porous tuffs with high fractions of capillary pores (e.g., CG, GF, ESC). The median value in the X direction (parallel to the bedding) of 53 tuffs is, with 9.7 kg/m$^2\sqrt{}$h, twice as high as in the Z direction (perpendicular to the bedding), with a median value of 5.0 kg/m$^2\sqrt{}$h. This clearly points to a better interconnection of the pore network along the bedding plane and is confirmed by the results of the water vapor

diffusion resistance (μ value), according to which the water vapor diffusion is noticeably aggravated in the Z direction (Table 3). The respective μ values, which were investigated for 50 tuffs, range from almost no diffusion resistances of 5.3 (SG1) to extremely high values of up 118.6 (CH), which practically indicate a diffusion barrier. In doing so, tuffs with low capillary water uptake obtain higher μ values and vice versa (Table 3).

The amount of water that a material can absorb from the air is displayed by the hygroscopic water sorption value. Due to their high porosity and specific surface area, some tuffs can obtain extreme water sorption potentials. Pötzl et al. (2021a) found increased hygroscopic water sorption especially in crystal tuffs with high amounts of swelling clays and zeolites and accordingly a high specific surface area (SSA), and decreased sorption values for vitric tuffs
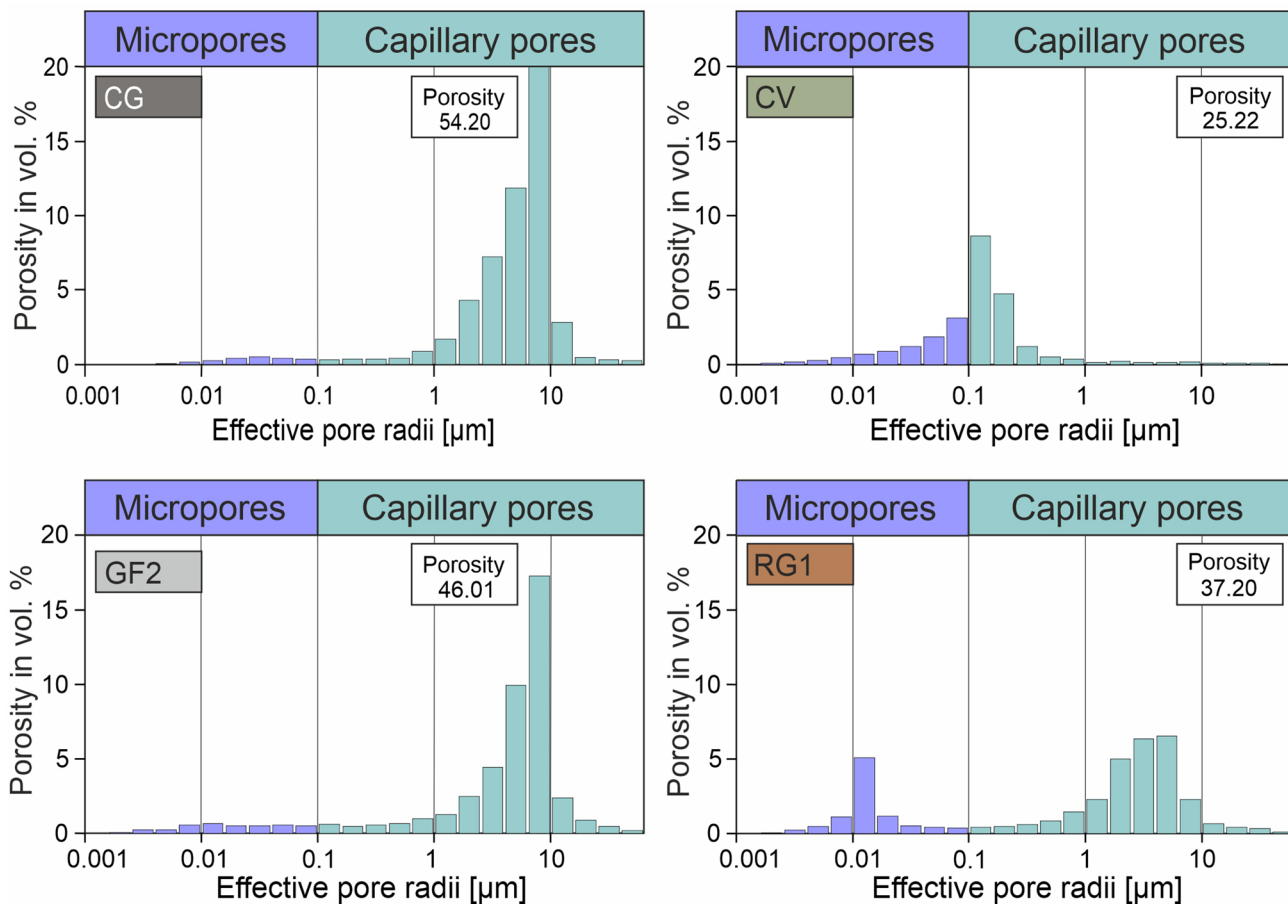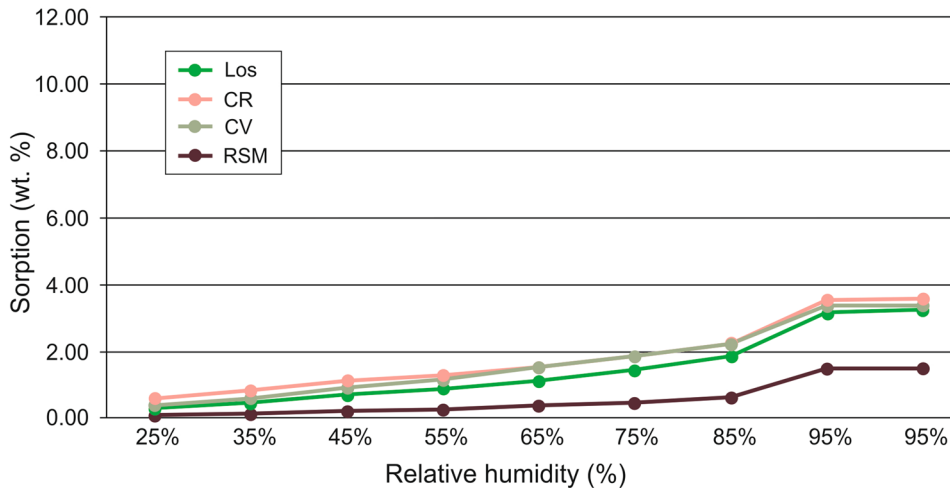
Fig. 10 Pore size distribution of selected tuffs from Mexico: samples CG, CV, GF2 and RG1

Fig. 11 Sorption curves for the Loseros (Los), Cantera Rosa (CR), Cantera Verde (CV) and the RSM tuff

with a low SSA. From 33 analyzed tuffs in this study, these overall trends can be partially confirmed. The Mexican tuffs experience a weight increase in the range of 0.4 wt% (ESC) up to 16.6 wt% (SG1), with a median of 2.6 wt%. Most tuffs show a significant weight increase in their adsorption curve at relative humidities of around 75% (Fig. 11). Highly hygroscopic active samples, like the SG and RG tuffs from San Miguel de Allende, exhibit significant hygroscopicity already at low humidity levels. Pötzl et al. (2021b) observed increasing hygroscopic water sorption on tuffs that were

pre-treated with a 1,4-diaminobutane dihydrochloride and explained this with the formation of hygroscopic salts, which are, due to their hygroscopic nature, known to efficiently adsorb moisture from the air (Steiger et al. 2011). The strong hygroscopicity of some tuffs in this study may be partly due to an increased salt load of the sample. Test specimens were not desalinated prior to the investigation and some of the sampled ashlars were utilized before in historical architecture for a considerable amount of time.

Mechanical properties

The strength of the Mexican tuffs in this study was characterized by both destructive and non-destructive measures. By means of the Brazil test, the tensile strength (TS) was characterized for 42 tuffs. The non-destructive measurement of the ultrasonic velocity was conducted on 51 tuffs. The TS values range between 0.6 and 15.0 mPa, and the ultrasonic velocities between 1.11 and 4.39 km/s. Low porous tuffs typically show higher TS and ultrasonic velocities (Table 3). Almost all tuffs show anisotropic behavior, especially the low porous tuffs, with higher TS and ultrasonic velocity in the X direction. While the median TS in the X direction is 2.7 mPa, the median TS in Z direction is 2.3 mPa. Both values are somewhat close to the median TS of 3.1 mPa that was found for a larger dataset of 150 volcanic tuffs in Pötzl et al. (2021a). The median ultrasonic velocity is 2.54 km/s in the X direction and 2.43 km/s in the Z direction.

The tensile strength under wet conditions was determined on thirteen tuffs of this study (Table 3). All 13 tuffs experience a strength reduction upon wetting, which can amount to a reduction of up to 70% (BP). The results confirm the findings of several studies that demonstrated a partly severe reduction in uniaxial compressive strength or tensile strength on water saturated tuffs (Çelik and Ergül 2015; Erguler and Ulusay 2009; Hashiba and Fukui 2015; Kleb and Vásárhelyi 2003; Masuda 2001; Okubo et al. 1992; Pötzl et al. 2021a; Török et al. 2004; Wedekind et al. 2013; Yasar 2020).

Hydric and thermal expansion

The hydric expansion of tuffs can exceed the values of other rock types by multiples (Pötzl et al. 2018a; Fig. 12). The Mexican tuffs of this study are no exception in this regard. The values range from barely any extension (0.01 mm/m for CHR, RSM, CG, TGQ) up to an extremely high extension of 7.8 mm/m (for rTF). An increased hydric expansion coincides with lower porosity and often with increased CEC and fraction of micropores. From 47 tuffs measured, the median of 0.28 mm in the Z direction is almost twice as high as in

the X direction (0.15 mm/m) indicating a strong directional dependence.

The coefficient of thermal expansion α was determined for 28 tuffs in this study and varies between 2.8×10^{-6} and 12.1×10^{-6} K^{-1}. The highest values are reached by tuffs with high amounts of quartz/glass. Similar to the hydric expansion, the Mexican tuffs show anisotropic behavior regarding their thermal expansion, with higher values in the Z direction (Table 3). A detailed discussion of influencing factors on the thermal expansion of Mexican tuffs can be found in López-Doncel et al. (2018).

Resistance against salt weathering

Tuffs may show highly differential behavior and resistance to salt crystallization processes, often depending on their mineralogy, pore radii distribution and expansional behavior (Çelik and Sert 2020; Germinario and Török 2019; López-Doncel et al. 2016; Pötzl et al. 2018a, b, 2021a; Yu and Oguchi 2010). Comprehensive data on the salt weathering of 17 volcanic tuffs from Mexico can be found in López-Doncel et al. (2016). Contrary to their observations, the tuffs investigated in this study do not show a clear correlation between their salt weathering resistance and their respective porosity or μ value. Instead, they typically show a decreasing resistance to salt weathering with increasing capillary water uptake, hygroscopic sorption and hydric expansion. The tuffs with unimodal unequal and bimodal pore radii distribution and a high fraction of micropores show higher susceptibility to salt weathering (Fig. 13), confirming the observations of recent studies on volcanic tuffs from Çelik and Sert (2020), Germinario and Török (2019), López-Doncel et al. (2016), Pötzl et al. (2018b), Pötzl et al. (2021a) and Yu and Oguchi (2010).

Concluding statements

The results of this investigation on the tuffs from Mexico, despite their strong heterogeneity, indicate some general trends and allow for some general statements regarding their technical properties and material behavior. The authors therefore directly formulate some observations and recommendations when dealing with this extremely diverse material, which may potentially help categorize the material and estimate weathering resistance and construction suitability. These statements are grouped below by subject:

General

1. In the dimensional stone industry, the collective term "tuff" or "Tuff Stone" is used to refer to a wide variety of

Fig. 12 Hydric expansion in different rock types. Modified from Pötzl (2020), after Kocher (2005) and references within
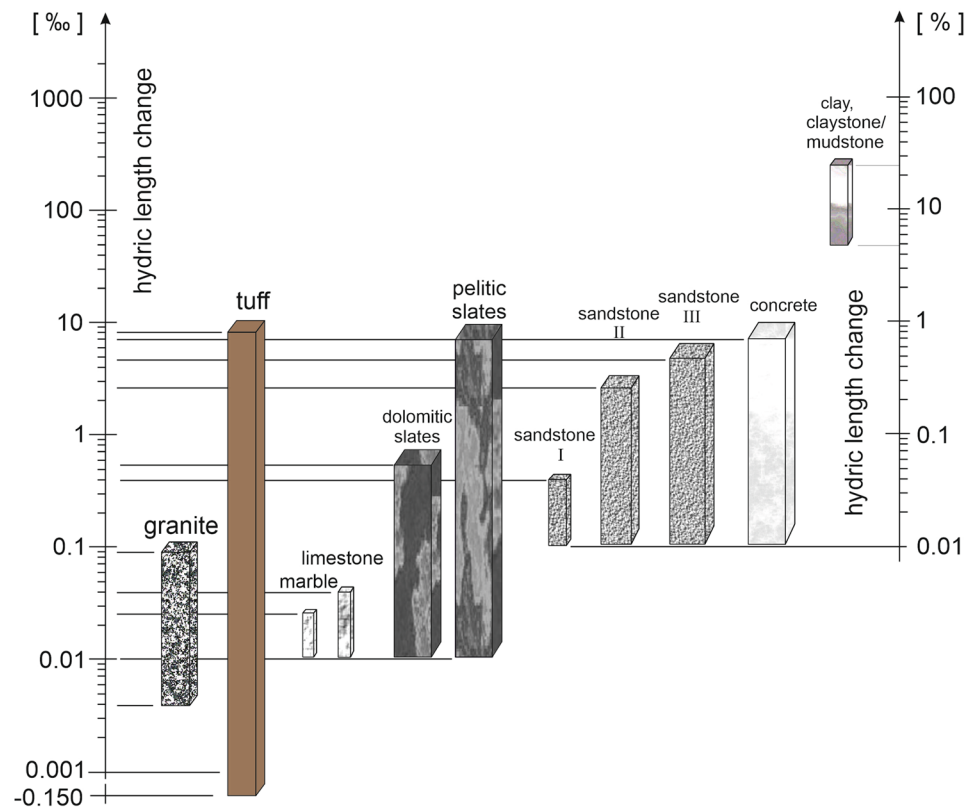
rock types that can differ significantly from one another in terms of fragmentation and deposition processes, types of particles, particle size, mineralogical composition, texture, etc.

2. Characterizing and predicting the material properties of "Tuff Stones" requires detailed investigations of their volcanic origin, petrographical, geochemical and petrophysical parameters.

3. Crystal, vitric and lithic tuffs show strongly differential characteristics in their technical parameters and consequently with regard to their durability.

Fabrics and mineralogical composition

4. One way to classify tuffs is according to the size and type of their pyroclastic fragments (Fischer 1966; Schmid 1981). The total alkali versus silica (TAS) classification system is commonly accepted for the geochemical classification of pyroclastic rocks, since the modal content of tuff cannot always be determined accurately with the QAPF diagram, due to the often cryptocrystalline and glassy texture of the groundmass.

5. As a result of the different geological formation and depositional processes, tuffs have very heterogeneous

and anisotropic rock fabrics, which can also be of a mineralogical nature with respect to the matrix and the rock fragments (pumice, lapilli, volcanic bombs). The anisotropic nature of tuffs is often expressed by a strong directional dependence of their technical parameters and weathering behavior. The arrangement of clay minerals within the stone fabrics for instance often results in an increased directional expansion perpendicular to the bedding plane.

6. As swelling rates of up to 7.8 mm/m are remarkable characteristic values for the hygric expansion of tuffs, and are undoubtedly discussed as damage-causing factors, not all types of tuff are characterized by a strong ability to expand. Investigations on their expansional behavior are, however, in any case recommended. The swelling rate of clay bearing tuffs should depend on the type and abundance of clay minerals and their local occurrence or local enrichment. Clay minerals represent a widespread mineral phase in these rocks. Their formation can be attributed to very different processes. The occurrence and distribution of clay minerals are variables depending on the rock genesis and alteration.

7. For tuffs several main occurrences of clay minerals can be distinguished. Primarily, clay minerals frequently

Fig. 13 Salt resistance test in four selected tuff stones from Mexico. Of the four depicted, only the Toba Rosa sample, an ignimbrite, shows the greatest resistance to salt weathering after 80 cycles

occur between grain contacts of larger detrital grains. Furthermore, clay minerals occur widely in lithoclasts, which are mostly distributed island-like in the rock body. In addition, clay minerals are frequently present in the form of clayey pore linings and fillings in tuffs, which are essentially a result of the alteration of vitric components. The latter can usually show a penetrative distribution into the rock.

8. Alteration of the tuffs leads to serpentinization and progressive chloritization of olivines. Plagioclases are albitized, sericitized or finally kaolinitized. The hydration of glass leads to the formation of the amorphous gel palagonite via various intermediate phases and finally, with progressive alteration, to clay minerals such as

smectite and montmorillonite or zeolite minerals. The latter is especially known to increase the amount of micropores, which may result in the increased potential for water adsorption and retention.

Petrophysical properties

9. Very important parameters to be taken into account are the hygric expansion, the water absorption, the porosity and especially the pore radii sizes, which have proven to have a great influence on the durability of tuffs. In terms of predicting these parameters for certain types of tuffs, correlations are rather unclear because of the very large heterogeneities.

10. The amount of water that a material can absorb from the air is displayed by the hygroscopic water sorption value. Due to their high porosity and specific surface area, some tuffs can obtain extreme water sorption potentials. Another technical parameter that displays the incredible water absorption potential of tuffs is the capillary water uptake, which usually is multiple times higher than that of other natural stones. Tuffs usually have a better interconnection of the pore network along the bedding plane. This is clearly displayed by the directional dependent capillary water uptake (w value) and vapor diffusion resistance (μ value), according to which the water uptake and vapor diffusion are noticeably aggravated perpendicular to the bedding.

11. Regarding their strength parameters, the strong anisotropic nature of tuffs is absolutely crucial to be taken into account when planning for their application. The partly severe reduction in material strength on water saturated tuffs is an often observed property of tuff and confirmed by this study. Some examples, especially crystal tuffs, experience a strength reduction upon wetting, which can amount to a reduction of up to 70% (e.g., sample BP).

12. Some trends can be inferred based on our very large sample collection from Mexico. Vitric tuffs exhibit the highest porosities, the largest mean pore sizes and higher capillary sorption values. The hygroscopic water sorption increases in crystalline tuffs and decreases in vitreous tuffs. The lowest and highest tensile strength data are found in vitric and crystal tuffs, respectively. Likewise, the lowest and highest ultrasonic velocities were measured in vitric and crystal tuffs, respectively. Regarding their hydric and thermal expansions, the highest values occur in crystal tuffs.

Damage, deterioration and conservation

13. This study confirms that the CEC is an overall good proxy for identifying the presence of swelling clay minerals in tuffs. However, the tuffs with the highest CEC do not necessarily show the highest expansion values, because not only the amount of expandable clay minerals are important but their position in the matrix. If such expandable clay minerals are located in open pores of a tuff rock, they can expand without building up any significant pressure. When located on crucial grain contacts, however, low expansion values may induce sufficient pressure to cause serious damage.

14. One aspect that according to our research plays a major role in both moisture, mechanical, and expansion properties is the crystallinity of the tuffs, so that the tendency is, the higher the crystallinity, the higher the initial stability of the tuff.

15. Depending on the environmental conditions, vitric or crystal tuffs may be more suitable for construction purposes. For example, vitric tuffs show a lower hydric expansion and higher salt weathering resistance on average, and therefore, may be the preferred material in humid environments, whereas crystal tuffs often show overall higher strength values, and may be the more durable material in arid environments.

16. For a more in-depth quality assessment, various aspects are extremely important since the weathering susceptibility of the tuffs can be derived from the exposure conditions and the prevailing environmental influences. The above statements also require the simultaneous analysis of the various petrophysical parameters as well as the complex effects on their common behavior. The exposition of the tuff controls the weathering behavior. Direct exposure to weathering creates different loading scenarios than exposure protected from rain or the influence of rising soil moisture as a result of contact with the ground. A permanent and high moistening requires different stone properties in terms of water storage, water transport and drying behavior.

17. Taking the Blanca Pachuca (BP), Toba Rosa (TR), El Salto (EIS) and Zacatecas (ZaC) tuffs as examples, the laboratory investigation has shown that these rocks have medium to strong suction properties. Moreover, these rocks have a very high percentage of capillary pores, which is much higher than 60%, except for the Toba Rosa (36%). These latter tuffs also belong to the highest porous rocks. The migration of foreign substances like salts or rising moisture would affect and control the weathering behavior, which can damage the structure.

18. If damage-causing substances occur, then frost weathering and salt weathering should also be taken into account. Toba Rosa has a lower porosity (11%), a very low S value (0.46) and few capillary pores that would be actively absorbent. During the salt weathering test, little damage is observed in the laboratory even after about 80 cycles, although the transition from thenardite to mirabilite is associated with a 314% increase in volume. Zacatecas and Blanca Pachuca show significant damage even before 20 salt cycles are reached.

19. Hygric swelling and shrinkage behavior are mainly controlled by the rapidly changing moisture or water contents. Since this involves cyclical repetitions (wetting/drying) and one-sided weathering, depending on the E-modulus of the tuffs, correspondingly high expansion pressures will occur in the case of hygric expansion. This can undoubtedly exceed the tensile strengths, and thus produce the damage pattern of spalling, flaking and peeling, etc.

20. The hygric and mechanical properties control the weathering characteristics and, in the case of restoration interventions, also the conservation behavior. Hygric swelling of more than one millimeter/meter should be regarded as a serious damage factor. Higher water absorption may well control higher swelling behavior, but higher humidity levels are already sufficient. The extreme heterogeneity with respect to the microstructures and mineralogical compositions of the tuffs do not allow any generally valid relationships.

21. The structural, microstructural and mineralogical heterogeneities result in considerable differences in hygric and mechanical properties, which in turn control the weathering properties and further define the approaches to conservation measures. Wrongly applied conservation measures, based on false predictions can significantly worsen the conservation status of the material.

Declarations

Conflict of interest The authors declare that there are no conflicts of interest.

References

Auras M, Egloffstein P, Steindlberger E (2000) Vulkanische Tuffsteine—Entstehung, Verwitterung, Konservierung. In: IFS Bericht, vol 10. Mainz, pp 35–52

Brooks Hanson R, Glazner AF (1995) Thermal requirements for extensional emplacement of granitoids. Geology 23:213–216

Bryan S (2007) Silicic large igneous provinces. Episodes 30:20

Bryan SE, Ferrari L (2013) Large igneous provinces and silicic large igneous provinces: progress in our understanding over the last 25 years. Geol Soc Am Bull 125:1053–1078

Bryan SE, Riley TR, Jerram DA, Stephens CJ, Leat PT, Menzies MA (2002) Silicic volcanism: an undervalued component of large igneous provinces and volcanic rifted margins. Special Papers-Geological Society of America, pp 97–118

Çelik MY, Ergül A (2015) The influence of the water saturation on the strength of volcanic tuffs used as building stones. Environ Earth Sci 74:3223–3239

Çelik MY, Sert M (2020) The role of different salt solutions and their concentration ratios in salt crystallization test on the durability of the Döğer tuff (Afyonkarahisar, Turkey) used as building stones of cultural heritages. Bull Eng Geol Environ. https://doi.org/10.1007/s10064-020-01896-7

Celik MY, Akbulut H, Ergül A (2014) Water absorption process effect on strength of Ayazini tuff, such as the uniaxial compressive strength (UCS), flexural strength and freeze and thaw effect. Environ Earth Sci 71:4247–4259

Columbu S, Gioncada A, Lezzerini M, Marchi M (2014) Hydric dilatation of ignimbritic stones used in the church of Santa Maria di Otti (Oschiri, northern Sardinia, Italy). Ital J Geosci 133:149–160

DIN 22024 (1989) Rohstoffuntersuchungen im Steinkohlenbergbau; Bestimmung der Spaltzugfestigkeit von Festgesteinen. Beuth, Berlin

DIN 66133 (1993) Bestimmung der Porenvolumenverteilung und der spezifischen Oberfläche von Feststoffen durch Quecksilberintrusion. Beuth, Berlin

DIN EN 772-4 (1998) Prüfverfahren für Mauersteine – Teil 4: Bestimmung der Dichte und der Rohdichte sowie der Gesamtporosität und der offenen Porosität von Mauersteinen aus Naturstein. Beuth, Berlin

DIN 13009 (2000) Bestimmung des hygrischen Dehnkoeffizienten. Beuth, Berlin

DIN EN ISO 12571 (2013) Bestimmung der hygroskopischen Sorptionseigenschaften. Beuth, Berlin

DIN EN ISO 12572 (2017) Bestimmung der Wasserdampfdurchlässigkeit. Beuth, Berlin

DIN EN ISO 15148 (2003) Bestimmung des Wasseraufnahmekoeffizienten bei teilweisem Eintauchen. Beuth, Berlin

DIN EN 14579 (2005) Prüfverfahren für Naturstein - Bestimmung der Geschwindigkeit der Schallausbreitung. Beuth, Berlin

Dohrmann R, Kaufhold S (2009) Three new, quick CEC methods for determining the amounts of exchangeable calcium cations in calcareous clays. Clays Clay Miner 57:338–352

Erguler ZA, Ulusay R (2009) Water-induced variations in mechanical properties of clay-bearing rocks. Int J Rock Mech Min Sci 46:355–370

Ferrari L, Orozco-Esquivel T, Manea V, Manea M (2012) The dynamic history of the Trans-Mexican Volcanic Belt and the Mexico subduction zone. Tectonophysics 522:122–149

DIN EN ISO 14581 (2014) Mechanische Verbindungselemente – Senk-schrauben mit Innensechsrund. Beuth, Berlin

DIN EN 12370 (2020) Prüfverfahren für Naturstein – Bestimmung des Widerstandes gegen Kristallisation von Salzen. Beuth, Berlin

Ferrari L, Orozco-Esquivel T, Bryan SE, Lopez-Martinez M, Silva-Fragoso A (2018) Cenozoic magmatism and extension in western Mexico: linking the Sierra Madre Occidental silicic large igneous province and the Comondú Group with the Gulf of California rift. Earth Sci Rev 183:115–152

Fisher RV (1966) Rocks composed of volcanic fragments and their classification. Earth Sci Rev 1:287–298

Fitzner B (1985) Bauforschung T2190/1. Ermittlung von Baust-offkennwerten von Tuffgesteinen und die Möglichkeiten zur Erhöhung der Dauerhaftigkeit von Tuffsteinmauerwerk-Teil 1. Fraunhofer IRB Verlag, Stuttgart

Germinario L, Török Á (2019) Variability of technical properties and durability in volcanic tuffs from the same quarry region–examples from Northern Hungary. Eng Geol 262:105319

Germinario L, Siegesmund S, Maritan L, Mazzoli C (2017) Petrophysical and mechanical properties of Euganean trachyte and implications for dimension stone decay and durability performance. Environ Earth Sci 76:739

Hashiba K, Fukui K (2015) Effect of water on the deformation and failure of rock in uniaxial tension. Rock Mech Rock Eng 48:1751–1761

Hildreth W (1981) Gradients in silicic magma chambers: implications for lithospheric magmatism. J Geophys Res 86:10153–10192

Hirschwald J (1912) Handbuch der bautechnischen Gesteinsprüfung für Beamte der Materialprüfungsanstalten und Baubehörden, Steinbruchingenieure, Architekten und Bauingenieure: sowie für Studierende der technischen Hochschulen, vol 2. Gebrüder Borntraeger

Jo YH, Lee CH (2022) Weathering features of a five-story stone pagoda compared to its quarrying site in Geumgolsan Mountain, Korea. Environ Earth Sci 81:1–13 (**In press**)

Kleb B, Vásárhelyi B (2003) Test results and empirical formulas of rock mechanical parameters of rhyolitic tuff samples from Eger's cellars. Acta Geol Hung 46:301–312

Kocher M (2005) Quelldruckmessungen und thermische Druckmessungen an ausgewählten Sandsteinen. Dissertation

Kück A, Pötzl C, López-Doncel RA, Dohrmann R, Siegesmund S (2020) Weathering behavior and petrophysical properties of the natural building stones used in the archeological site of Mitla and colonial buildings in Oaxaca, Mexico. In: Siegesmund S, Middendorf B (eds) Monument future: decay and conservation of stone, 1st edn. Mitteldeutscher Verlag, Halle

López-Doncel R, Wedekind W, Dohrmann R, Siegesmund S (2013) Moisture expansion associated to secondary porosity: an example of the Loseros Tuff of Guanajuato, Mexico. Environ Earth Sci 69:1189–1201

López-Doncel R, Wedekind W, Leiser T, Molina-Maldonado S, Velasco-Sánchez A, Dohrmann R, Kral A, Wittenborn A, Aguillón-Robles A, Siegesmund S (2016) Salt bursting tests on volcanic tuff rocks from Mexico. Environ Earth Sci 75:212

López-Doncel R, Wedekind W, Aguillón-Robles A, Dohrmann R, Molina-Maldonado S, Leiser T, Wittenborn A, Siegesmund S (2018) Thermal expansion on volcanic tuff rocks used as building stones: examples from Mexico. Environ Earth Sci 77:338

López Luján L, Torres J, Montúfar A (2003) Los materiales constructivos del Templo Mayor de Tenochtitlán. Estudios De Cultura Nahuatl 34:137–167

Machel HG, Mason RA, Mariano AN, Mucci A (1991) Causes and emission of luminescence in calcite and dolomite. In: Barker CE, Kopp OC (eds) Luminescence microscopy and spectroscopy: qualitative and quantitative applications, Soc Sed Geol, pp 9–25

Marshall DJ (1988) Cathodoluminescence of geological materials. Unwin Hyman, Boston

Masuda K (2001) Effects of water on rock strength in a brittle regime. J Struct Geol 23:1653–1657

McDowell FW, Keizer RP (1977) Timing of mid-Tertiary volcanism in the Sierra Madre Occidental between Durango city and Mazatlán, Mexico. Geol Soc Am Bull 88:1479–1487

Meier L, Kahr G (1999) Determination of the cation exchange capacity (CEC) of clay minerals using the complexes of copper (II) ion with triethylenetetramine and tetraethylenepetamine. Clays Clay Miner 47:386–388

Mora-Navarro G, López-Doncel RA, Espinosa Pesqueira M, Wedekind W (2016) Weathering and deterioration of building stones in Templo Mayor, Mexico City. Science and Art: a future for stone. In: Proceedings of 13th International Cong on Deterioration and Conservation of Stone, I: 117–124, Glasgow, ISBN: 978-1-903978-59-7

Mori L, Gómez-Tuena A, Schaaf P, Goldstein SL, Pérez-Arvizu O, SolÍs-Pichardo G (2009) Lithospheric removal as a trigger for flood basalt magmatism in the Trans-Mexican Volcanic Belt. J Petrol 50:2157–2186

Navarro GM, Doncel RL, Pesqueira ME, Wedekind W (2016) Weathering and deterioration of building stones in Templo Mayor, Mexico City. In: Hughes JJ, Howind T (eds) Science and art: a future for stone. pp 117–124

Neuser RD, Bruhn F, Habermann D, Richter DK (1995) Kathodolumineszenz: Methodik und Anwendung. Zbl Geol Paläont Teil I H 1(2):287–306

Okubo S, Nishimatsu Y, He C, Chu SY (1992) Loading rate dependency of uniaxial compressive strength of rock under water-saturated condition. Zairyo 41:403–409

Padilla Sánchez RJ (2017) Tectonic Map of Mexico GIS Project. Am Assoc Petrol Geol. https://doi.org/10.13140/RG.2.2.35486.33608 (**GIS Open Files series**)

Pasquarè G, Ferrari L, Covelli P, Agostini G de (1991) Geologic map of the central sector of the Mexican Volcanic Belt, states of Guanajuato and Michoacan, Mexico. Geol Soc Amer

Pötzl C (2020) Volcanic tuffs as natural building stones: Mineralogy, technical properties, deterioration and conservation strategies. Dissertation, Georg-August-University

Pötzl C, Siegesmund S, López-Doncel R, Wedekind W (2016) Las Casas Tapadas de Plazuelas-structural damage, weathering characteristics and technical properties of volcanic rocks in Guanajuato, Mexico. In: Hughes JJ, Howind T (eds.) Science and art: a future for stone, vol II. pp 1237–1245

Pötzl C, Dohrmann R, Siegesmund S (2018a) Clay swelling mechanism in tuff stones: an example of the Hilbersdorf Tuff from Chemnitz, Germany. Environ Earth Sci 77:188

Pötzl C, Siegesmund S, Dohrmann R, Koning JM, Wedekind W (2018b) Deterioration of volcanic tuff rocks from Armenia: constraints on salt crystallization and hydric expansion. Environ Earth Sci 77:660

Pötzl C, Rucker S, Wendler E, Siegesmund S (2021a) Consolidation of volcanic tuffs with TEOS and TMOS: a systematic study. Environ Earth Sci. https://doi.org/10.1007/s12665-021-10066-1 (**In Press**)

Pötzl C, Siegesmund S, López-Doncel R, Dohrmann R (2021b) Key parameters of volcanic tuffs used as building stone: a statistical approach. Environ Earth Sci. https://doi.org/10.1007/s12665-021-10114-w (**In Press**)

Ruedrich J, Bartelsen T, Dohrmann R, Siegesmund S (2011) Moisture expansion as a determination factor for sandstone used in buildings. Environ Earth Sci 63:1545–1564

Rucker S, Pötzl C, Wendler E, Dohrmann R, López-Doncel RA, Siegesmund S (2020) Improved consolidation of volcanic tuff rocks with TEOS. In: Siegesmund S, Middendorf B (eds) Monument future:

decay and conservation of stone, 1st edn. Mitteldeutscher Verlag, Halle

Ruedrich J, Siegesmund S (2006) Fabric dependence of length change behaviour induced by ice crystallisation in the pore space of natural building stones. In: Heritage, weathering and conservation: proceedings of the international conference on heritage, weathering and conservation. Taylor & Francis, pp 497

Schmid R (1981) Descriptive nomenclature and classification of pyroclastic deposits and fragments: recommendation of the IUGS Subcommission on the systematics of igneous rocks. Geol 9:41–43

Sieck P, López-Doncel R, Dávila-Harris P, Aguillón-Robles A, Wemmer K, Maury RC (2019) Almandine garnet-bearing rhyolites associated to bimodal volcanism in the Mesa Central of Mexico: geochemical, petrological and geochronological evolution. J South Am Earth Sci 92:310–328

Siegesmund S, Dürrast H (2011) Physical and mechanical properties of rocks. In: Siegesmund S, Snethlage R (eds) Stone in Architecture. Springer, Berlin, pp 97–225

Steiger M, Charola AE, Sterflinger K (2011) Weathering and deterioration. In: Siegesmund S, Snethlage R (eds) Stone in architecture. Springer, Berlin, pp 227–316

Steindlberger E (2003) Vulkanische Gesteine aus Hessen und ihre Eigenschaften als Naturwerksteine. Teilw. zugl.: Frankfurt am Main, Univ., Diss., 2002 u.d.T.: Steindlberger, E.: Untersuchungen zum physiko-chemischen Verwitterungsverhalten hessischer Tuffsteine. Geologische Abhandlungen Hessen, vol 110. HLUG, Wiesbaden

Swanson ER, McDowell FW (1984) Calderas of the Sierra Madre occidental volcanic field western Mexico. J Geophys Res 89:8787–8799

Török A, Gálos M, Kocsányi-Kopecskó K (2004) Experimental weathering of rhyolite tuff building stones and the effect of an organic polymer conserving agent. Stone decay: its causes and controls, pp 109–127

Török A, Forg LZ, Vogt T, Löbens S, Siegesmund S, Weiss T (2007) The influence of lithology and pore-size distribution on the durability of acid volcanic tuffs, Hungary. Geol Soc Lond Spec Publ 271:251–260

Török A, Germinario L, Lopez-Doncel R, Pötzl C, Siegesmund S (2020) Comparative analysis of volcanic tuffs from Europe, Asia and North-America. In: Siegesmund S, Middendorf B (eds) Monument future: decay and conservation of stone, 1st edn. Mitteldeutscher Verlag, Halle, pp 131–136

Ufer K, Kleeberg R, Bergmann J, Dohrmann R (2012) Rietveld refinement of disordered illite-smectite mixed layer structures by a recursive algorithm. II: powder-pattern refinement and quantitative analysis. Clays Clay Miner 60:535–552

Wark DA (1991) Oligocene ash flow volcanism, northern Sierra Madre Occidental: Role of mafic and intermediate-composition magmas in rhyolite genesis. J Geophys Res Solid Earth 96:13389–13411

Wedekind W, Ruedrich J, Siegesmund S (2011) Natural building stones of Mexico–Tenochtitlán: their use, weathering and rock properties at the Templo Mayor, Palace Heras Soto and the Metropolitan Cathedral. Environ Earth Sci 63:1787–1798

Wedekind W, López-Doncel R, Dohrmann R, Kocher M, Siegesmund S (2013) Weathering of volcanic tuff rocks caused by moisture expansion. Environ Earth Sci 69:1203–1224

Yasar S (2020) Long term wetting characteristics and saturation induced strength reduction of some igneous rocks. Environ Earth Sci 79:1–12

Yu S, Oguchi CT (2010) Role of pore size distribution in salt uptake, damage, and predicting salt susceptibility of eight types of Japanese building stones. Eng Geol 3:226–236